Chapter 4

Unraveling the Hidden Nature of Antenna Excitations

Arvi Freiberg*
Institute of Physics, University of Tartu, Riia 142, 51014 Tartu, Estonia and Institute of Molecular and Cell Biology, University of Tartu, Riia 23, 51010 Tartu, Estonia

Gediminas Trinkunas
Institute of Physics, Savanoriu 231, LT-02300 Vilnius, Lithuania

Summary

The three main parameters that determine the electronic structure and dynamics of the photosynthetic antenna excitations are the resonant (exciton) coupling energy, the inhomogeneous spectral broadening, and the exciton–lattice coupling energy. Generally, information about these factors can be obtained by optical spectroscopy. However, in conventional optical spectroscopy only ensemble-averaged data are accessible. Adequate theoretical modeling is, therefore, required to uncover various hidden parameters. Here, we focus on the peripheral LH2 and core LH1 antenna complexes from purple bacteria. These bacteriochlorophyll-containing antennas show quasi-linear optical spectra that allow detailed spectroscopic studies not only at cryogenic temperatures but at physiological temperatures as well. The strongly overlapping chlorophyll spectra in higher plant antennas are in that respect much less informative. Secondly, the bacterial antennas present wonderfully ordered quasi- one-dimensional structures of pigment molecules amenable for straightforward physical modeling. Complexity of the antennas and incomplete structural data render similar level of multi-parameter modeling in higher plants more challenging.

* Author for correspondence, e-mail: Arvi.Freiberg@ut.ee

A. Laisk, L. Nedbal and Govindjee (eds.), Photosynthesis in silico: Understanding Complexity from Molecules to Ecosystems, pp. 55–82.

We notice that the generally applied disordered Frenkel exciton model, while sufficient for describing steady-state absorption spectra, falls short in characterization of the fluorescence emission properties of the bacterial antennas. Therefore, an excitonic polaron model is introduced, much better suitable for description of the relaxed excited electronic states in the disordered one-dimensional bacteriochlorophyll aggregates representing the emitting antenna structures with relatively strong interaction between excitons and lattice vibrations. The static disorder considerably reduces critical exciton–lattice coupling energy required for initiation of the smooth exciton self-trapping transition. It also allows coexistence of multiple self-trapped excitons in the same lattice. Such a situation in regular structures is only possible at higher dimensions. The exciton self-trapping might promote energy transport and trapping processes in bacterial photosynthesis by broadening the LH2 and LH1 antenna spectra and by maximizing their fluorescence emission rate.

I. Introduction

A. Light Harvesting

Photosynthesis utilizes two coupled pigment systems, a light-harvesting (LH) antenna and a photochemical reaction center, cooperating in conversion of solar energy into chemically stable high-energy products sustaining life on Earth. Together, the antenna and the reaction center form an entity called photosynthetic unit, the concept first introduced in the beginning of 1930s (Emerson and Arnold, 1932) to explain efficiency of the photosynthetic solar energy conversion. L. N. M. Duysens and collaborators (Duysens, 1952; Vredenberg and Duysens, 1963) provided an early experimental proof of this concept by spectroscopic means. Subsequent biochemical studies revealed further complexity with different pigment-protein complexes performing the antenna and reaction center functions. Detailed research on molecular level vastly expanded our understanding of the photosynthetic apparatus and its functioning with new insights provided by the high-resolution crystallographic characterization of the bacterial photosynthetic reaction center (Michel and Deisenhofer, 1990) as well as of a number of LH units of both bacterial (Fenna and Matthews, 1975; McDermott et al., 1995; Koepke et al., 1996) and higher plant origin (Loll et al., 2005; Amunts et al., 2007). By now, it is firmly established for all photosynthetic organisms that the LH antenna proteins are composed of a large number of pigment molecules. Their task is to collect sunlight and deliver energy to the reaction center protein. The latter, by contrast, comprise only a few pigment molecules, whose organization and interactions are optimized for unidirectional electron transfer across the photosynthetic membrane leading to a long-lived charge separation state. The turnover time of the reaction centers is much shorter than intervals between its photon capture. The additional light harvesting by antenna structures is increasing the photon capture frequency and, thus, increasing the efficiency of the photosynthetic unit by several orders of magnitude. Further enhancement is achieved by broadening spectral range of the light harvesting above that of the reaction center only.[1]

B. Irregular Pigment Organization and the Energy Funneling Principle

The most abundant LH complexes are composed of different forms of chlorophyll or bacteriochlorophyll molecules that are non-covalently bound to the surrounding protein matrix. Structural studies give evidence for complex spatial pattern of the pigments. In all known antenna complexes, the densely packed pigment constellations (including dimers, trimers, and larger oligomers of up to thousand molecules) interlace with scarcely occupied regions. The spatial heterogeneity is not accidental. It was demonstrated in a series of modeling papers (Fetisova

Abbreviations: Bchl – bacteriochlorophyll *a*; DOS – density of states; FLN – fluorescence line narrowing; FWHM – full width at half maximum; LH – light-harvesting; PSB – phonon sideband; SDF – site/state distribution function; ZPL – zero phonon line; 1D, 2D, 3D – one-, two-, three-dimensional

[1] This unique principle of natural photosynthesis has lately been introduced into modern photovoltaic technology (see Markvart, 2000 for a review).

et al., 1985, 1989; Fetisova, 2004) that the clustered antenna structure increases efficiency of the delivery of excitations from the antenna to the reaction center compared with that of a system with uniform distribution of the pigments.

The spatial structure of the antenna complexes, especially the mutual orientation of the pigments, also determines to a large extent their spectroscopic properties and excited-state dynamics. High local concentration of the pigments, favoring extensive inter-pigment couplings, causes coherent de-localization of the excited states over at least a part of the cluster. Therefore, as first realized already 70 years ago (Franck and Teller, 1938), delocalized Frenkel excitons (Knox, 1963; Davydov, 1971) rather than excited states of individual molecules are relevant electronic excitations for the densely packed arrays of the antenna pigments. It, however, took hard work and determination of several generations of scientists (Robinson, 1967; Sauer and Austin, 1978; Pearlstein, 1982; Scherz and Parson, 1986; Novoderezhkin and Razjivin, 1993, 1995) until the exciton concept in photosynthesis has been generally accepted (Van Amerongen et al., 2000). The progress made in high-resolution structural studies of LH complexes of purple bacteria (Karrasch et al., 1995; McDermott et al., 1995; Koepke et al., 1996; Walz et al., 1998; McLuskey et al., 2001) has strongly stimulated these investigations (Jimenez et al., 1996; Sauer et al., 1996; Scholes et al., 1997, 1999; Wu et al., 1997b; Sumi, 1999a, b, 2000; Sundström et al., 1999; Van Oijen et al., 1999; Scholes and Fleming, 2000; Green and Parson, 2003; Hu et al., 2002; Van Grondelle and Novoderezhkin, 2006).

Excitons are scattered by various structural irregularities (generally called disorders) that exist in the assembly of molecules. Relative to the exciton lifetime or to the time-window of the measurement these irregularities are static or dynamic (time dependent). The static and dynamic disorders produce spectral line broadening called inhomogeneous and homogenous broadening, respectively. Thermal fluctuations in the positions of atoms and molecules mediated by electron–phonon[2] coupling are the main cause of the homogeneous broadening of the exciton spectra (Mukamel, 1995; Renger and Marcus, 2002; Heijs et al., 2005). In contrast to, for example, molecular crystals, the excitons in pigment-proteins are affected both in nature and dynamics by physical size and structure of these complexes (Sumi, 2000; Scholes and Rumbles, 2006). A very large inhomogeneous line-broadening characteristic for nano-particle type pigment-proteins may even obscure their exciton features. This certainly was one of the main factors slowing down the progress of recognizing excitons in the photosynthetic antennas.

In the antenna pigment-protein complexes, it is worth distinguishing between spectral inhomogeneity and spectral heterogeneity (Pullerits et al., 1994). The heterogeneity is a result of large-scale systematic differences in the surroundings of the pigment molecules (e.g., due to binding to different polypeptides or to different parts of a polypeptide chain), while the inhomogeneity is caused by small, random fluctuations in the positions and orientations of the pigment molecules. The heterogeneity results in the absorption spectrum in more or less distinct lines or bands, which can be attributed to spatially distinct groups of the pigments in the antenna structure as shown in Fig. 4.1.

In the spectroscopy of organic impurity crystals such combination of the inhomogenous

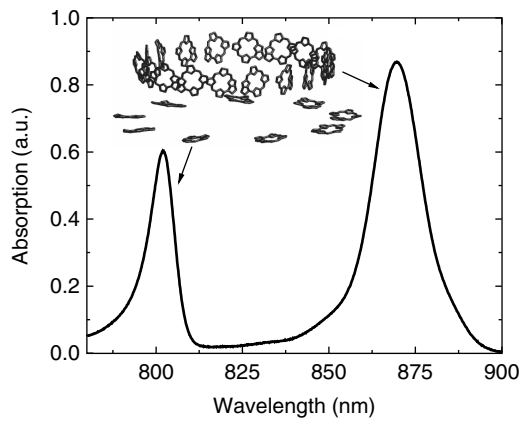

Fig. 4.1. Relationship between the structural arrangement of the Bchl molecules in the LH2 light-harvesting complex from the purple bacterium *Rps. acidophila* and their absorption spectra in the near-infrared region at 5 K. The Bchl molecules are represented by their bacteriochlorin cores. The B850 absorption band corresponding to the closely spaced upper-ring molecules (B850 is a conventional term, here the band is at 868 nm in *Rps. acidophila*) is the main focus of this work

[2] The term "phonon" in this text is loosely assigned to any vibrational motion, extended or localized, if not otherwise indicated.

and heterogenous broadenings is known as the Shpol'skii effect (Gooijer et al., 2000).

A spatially ordered arrangement of different spectral forms of the pigments in the heterogeneous antennas improves the photosynthetic unit efficiency if the groups of the antenna pigments are spatially organized with respect to the reaction center in a way that an energy gradient is created driving the excitation energy toward the reaction center (Duysens, 1986). The green photosynthetic bacteria as well as cyanobacteria, which contain extra-membranous accessory antenna complexes (chlorosomes and phycobilisomes, respectively), are the two archetypical representatives of such a funnel type antenna arrangement (Porter et al., 1978; Fetisova et al., 1988, 1995). The same principle facilitates effective exciton transfer also in the purple bacteria (Freiberg et al., 1987; Godik et al., 1988; Pullerits and Freiberg, 1991; Freiberg, 1995).

C. Light Harvesting by Purple Photosynthetic Bacteria

The photosynthetic membrane of many purple bacteria contains two types of LH complexes, the core LH1 and the peripheral LH2 complex. The LH1 complex directly surrounds the reaction center (Karrasch et al., 1995; Walz et al., 1998; Roszak et al., 2003; Bahatyrova et al., 2004), whereas LH2, usually not in straight contact with the reaction center, transfers its energy to the reaction center via the core complex (Sundström et al., 1999; Hu et al., 2002; Cogdell et al., 2006). Both LH1 and LH2 contain a remarkable circular assembly of the light-harvesting pigments in their protein matrix. The basic building block of these structures is a heterodimer of a α- and β-apoproteins. The whole LH2 complex consists of either nine (*Rhodopseudomonas (Rps.) acidophila, Rhodobacter (Rb.) sphaeroides*) (McDermott et al., 1995) or eight (*Rhodospirillum (Rs.) molischianum*) (Koepke et al., 1996) such αβ-heterodimers, each non-covalently binding three bacteriochlorophyll *a* (BChl) molecules and one carotenoid molecule. The LH1 complex from *Rb. sphaeroides* consists of 16 αβ-heterodimers (Walz et al., 1998), each binding two Bchl molecules and one or two carotenoid molecules.

The arrangement of Bchl molecules in the LH2 complex from *Rps. acidophila* (McDermott et al., 1995) and the related absorption spectrum are shown in Fig. 4.1. A striking feature of the organization of the 27 Bchl molecules in this LH2 complex is their partition into two concentric rings. The upper ring consists of a group of 18 closely coupled (intermolecular separation <1 nm) Bchls with their bacteriochlorin planes oriented parallel to the vertical symmetry axis of the complex. These molecules give rise to absorption around 850–870 nm (different in different species) named as the B850 band. The nine loosely packed Bchls (intermolecular distance ≥ 2 nm) in the lower ring are responsible for the B800 absorption band. These molecules have their bacteriochlorin planes perpendicular to the symmetry axis.

A single-ring arrangement of the Bchls in LH1 reminds that in the upper circle of LH2. These strongly coupled pigments give rise to an absorption in the 875 nm region. All the three spectral bands (B800, B850, and B875) of the LH1 and LH2 antenna complexes originate in the lowest Q_y singlet electronic transition.

Upon excitation, the energy is funneled from B800 to B850 molecules in 1–2 ps (Sundström et al., 1986; Godik et al., 1987; Van Grondelle et al., 1987; Freiberg et al., 1989; Shreve et al., 1991). Subsequent electronic energy transfer from LH2 to LH1, i.e., between the B850 and B875 antenna rings, is less uniform (Nuijs et al., 1986; Sundström et al., 1986; Godik et al., 1987, 1988; Freiberg et al., 1989). In wild type membranes (chromatophores) of *Rb. sphaeroides*, for example, most (∼70%) of the LH2 excitations carry their energy to LH1 very fast, in less than 10 ps, while the rest are much delayed, taking about 50 ps (Godik et al., 1987; Freiberg et al., 1988, 1989). It was proposed that those of the LH2 complexes that exhibit restrained transfer rate, must lie in a periphery of the antenna cluster (Godik et al., 1987; Freiberg et al., 1989; Zhang et al., 1992). The proposed antenna pattern, with some remote LH2 and some LH2 that are directly coupled to LH1, is remarkably similar to the antenna topology discovered more than a decade later by atomic force microscopy (Scheuring, 2006).

The overall (quasi-equilibrium) lifetime of excitations in intact membranes with the reac-

tion centers in the photoactive state is 50–70 ps (Borisov and Godik, 1972; Godik and Borisov, 1977; Sebban and Moya, 1983; Freiberg et al., 1984; Sebban et al., 1984; Borisov et al., 1985; Dobek et al., 1990). There is a general consensus that this lifetime is primarily limited by the slow rate of energy transfer from the core LH1 antenna to the reaction center trap (see Zhang et al., 1992; Timpmann et al., 1993; Beekman et al., 1994; Timpmann et al., 1995; Freiberg et al., 1996; Katiliene et al., 2004 for relevant discussions).

The experimentally confirmed ultrafast excitation energy funneling toward the reaction center assigns special role to the densely packed B850 and B875 rings of Bchls. Characterized with the lowest electronic transition energies in the respective LH2 and LH1 complexes, they govern the functionally important flow of the solar excitation energy in the photosynthetic membranes of purple bacteria. Our aim in this chapter is not only a better qualitative understanding of the origin of the lowest electronic excited states of the B850 and B875 pigment aggregates, but also a quantitative evaluation of the main physical parameters related to this origin. The study is based on theoretical analysis and numerical simulations of the steady-state conventional and selective spectroscopy data obtained on ensembles of disordered LH2 and LH1 complexes at low temperatures. As a convention, the term "selective" will be used to denote excitation of an electronic state within its inhomogeneously broadened origin band. Such excitation results in line-narrowed fluorescence (FLN) and absorption (hole burning) spectra. Since high-resolution structural information is available only for the peripheral LH2 antenna complex, the main discussion is based on the B850 aggregate. However, most of the results are applicable for the B875 aggregate as well.

II. Disordered Frenkel Exciton Model for Absorbing States of Circular Antenna Aggregates

The X-ray structure of *Rps. acidophila* refined to a resolution of 0.2 nm (Papiz et al., 2003) shows distances close to 0.87 nm between the central Mg atoms of the Bchls in the B850 basic unit and only slightly larger space of 0.97 nm between the adjacent units. Close arrangement and large dipole strength of the Q_y electronic transition give rise to significant resonant interactions between the neighboring Bchls that readily distribute (delocalize) the excited states over at least part of the B850 molecules. Hence, a natural starting point to describe the excited states of the B850 assembly is by applying the Frenkel exciton model (Davydov, 1971). In its idealized form (without static and dynamic disorders taken into account), the key aspects of this model are as follows (Van Amerongen et al., 2000). The proper exciton eigenstates are characterized by a quantum number, k, which can take the values $0, \pm1, \pm2, \ldots, \pm8, 9$. Owing to the circular symmetry and tangential orientation of the transition dipoles of the Bchl molecules almost on the B850 ring plain, only the states $k = \pm1$ carry an appreciable transition-dipole moment, making them easily accessible by ground-state absorption spectroscopy. The symmetric $k = \pm8$ states at the upper-energy edge of the exciton state manifold are very weak, whereas the remaining 14 states are inaccessible from the ground state. These strict optical selection rules in regular aggregates are characteristic for the delocalized exciton states and result from the fact that the exciton wavefunctions are the Bloch states that span over the whole molecular structure. In addition, the exciton states of the B850 aggregate are influenced by a periodic dimeric organization of the Bchl molecules in the ring imposed by the supporting α- and β-apoproteins (Liuolia et al., 1997).[3] Because of that, a site excitation energy difference for the neighboring Bchls appears together with two nearest-neighbor exciton coupling energies, V and V'. Their ratio estimated in the dipole–dipole coupling approximation from the X-ray structure (Papiz et al., 2003) is $V'/V \approx 0.76$. The exciton band that is $2(V + V')$ broad is split into two Davydov subbands, separated by a bandgap of $2(V - V')$. As can be seen in Fig. 4.2a (central bars), each Davydov subband comprises of four pair-wise degenerate exciton states and one non-degenerate state at either the low-energy or the high-energy edge.

[3] Making connection with the solid-state physics terminology: there are two molecules per unit cell of the ring structure.

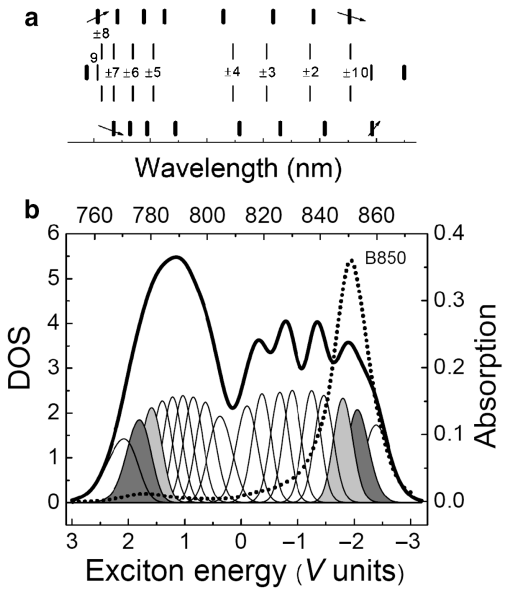

Fig. 4.2. Panel **a:** excitonic level diagrams for regular (central thin bars) and diagonally disordered (flank thick bars) B850 aggregates. The arrows indicate transition dipole moments for the disorder-split k $= \pm 1$ and k $= \pm 8$ exciton states. A single diagonal disorder realization of site energies from a Gaussian distribution (see Eq. 4.2) with $\sigma = 0.6V$ is represented. Panel **b:** the absorption spectrum (dotted curve) and the corresponding DOS (thick curve) for an ensemble of 2000 B850 aggregates. The shapes drawn with thin line represent ensemble distributions of 18 individual exciton states. The filled gray areas highlight the distributions for the split k $= \pm 1$ and k $= \pm 8$ states. The model parameters suitable for LH2 from *Rb. sphaeroides* have been used in these calculations

Certain amount of static structural disorder exists in all proteins. As already indicated, these fluctuations lead to heterogeneous and inhomogeneous spectral line broadening. The low-temperature persistent hole burning studies of Small and Völker (Van der Laan et al., 1990; Reddy et al., 1992) provided the first clear proof that the B800, B850, and B875 bands are inhomogeneously broadened. These data nicely corroborated the indirect evidence that was obtained previously from picosecond time-resolved measurements (Freiberg et al., 1987, 1989; Zhang et al., 1992). More recently, the large variability of the antenna spectra both at cryogenic and physiological temperatures was affirmed by single complex studies (Tietz et al., 1999; Van Oijen et al., 1999). In hole burning spectroscopy, an intense, narrow bandwidth laser selects a sub-population of chromophores in the inhomogeneous absorption band. Photochemical and/or photophysical processes cause bleaching of the chromophores resonant with the laser frequency. While the photochemical mechanism acts directly on the chromophores, the photophysical mechanism is believed to modify only the environment of the chromophores. The missing absorption at excitation frequency appears as nearly homogenously broadened inverted spectral profile, a hole, in the inhomogeneous absorption band. The narrow spectral holes burned in the low-energy region of the LH2 and LH1 absorption spectra failed to spot any significant phonon sidebands (Van der Laan et al., 1990; Reddy et al., 1992). This was taken (erroneously, as we shall see shortly) as a proof of a rather weak coupling between the pigment molecules and the surrounding protein matrix (below referred to as electron– or exciton–phonon coupling), promoting the disordered Frenkel exciton approach for the photosynthetic excitations.

As follows, a disordered Frenkel exciton model is introduced in relation with absorption spectra of the B850 aggregates. In this model, perturbations of the exciton states by static variances of the Q_y transition energies and coordinates of individual Bchl molecules are considered more significant than the dynamic disorder due to vibrating protein and pigment nuclei. Since the results of this theory are widely known (Jimenez et al., 1996; Wu et al., 1997a; Novoderezhkin et al., 1999), only those of its aspects will be discussed that are needed to understand the fluorescence emission anisotropy measurements of the LH2 complexes as a function of the excitation wavelength (Timpmann et al., 2004a). In these experiments, the edges of the exciton state manifold corresponding to the $k = \pm 1$ and $k = \pm 8$ states were probed. Hence, the width of the B850 exciton band and the corresponding exciton coupling energies could be first reliably estimated. Similar studies for the LH1 complex (i.e., the B875 aggregate) were performed in (Timpmann et al., 2005).

The rigid-lattice exciton Hamiltonian, which takes into account both diagonal (or energetic),

$\delta\varepsilon_n$, and off-diagonal (or structural), δt_{nm}, disorders reads[4]

$$H_0 = \sum_{n=1}^{N} (\varepsilon_0 + \delta\varepsilon_n) \, |n\rangle\langle n| + \sum_{n,m=1;n\neq m}^{N} (t_{nm} + \delta t_{nm} \, |n\rangle\langle m|). \quad (4.1)$$

Here, $|n\rangle$ and $\langle n|$ represent the ket and bra vectors, respectively, for the excitation that is localized on the n-th Bchl molecule (shortly, on site n), N is the total number of the sites, and t_{nm} denotes the intermolecular coupling energy between the sites n and m ($n \neq m$). Physically, the first sum in Eq. (4.1) relates to the individual molecular excitations, while the second term accounts for the electronic couplings between the molecules. The latter couplings are mediated by the Coulomb interactions of the electrons and nuclei whose leading contribution is the transition dipole–dipole term. Due to the achieved resonance of the transition frequencies the molecular excitations start moving around, in principle covering the whole aggregate. The maximal absolute value of the coupling, $V = \max\{|t_{nm}|\}$ (corresponding to the $\alpha\beta$ intra-dimer coupling in the LH2 structure of *Rps. acidophila*), is in the following computations utilized as an energy unit.

The Q_y excited state energies, ε_n, of the Bchls are assumed to be random variables distributed according to the normal law, $P(\varepsilon_n)$, with the mean, ε_0, and the standard deviation, σ[5]:

$$P(\varepsilon_n) = \frac{1}{\sqrt{2\pi\sigma^2}} \exp\left(-\frac{(\varepsilon_n - \varepsilon_0)^2}{2\sigma^2}\right). \quad (4.2)$$

Equation (4.2) thus constitutes the diagonal disorder model, where $\varepsilon_n = \varepsilon_0 + \delta\varepsilon_n$. As for the off-diagonal model, there are many ways how the structural disorder can be implemented (Jang et al., 2001). For example, one could distribute the Bchl distances, R_n, from the symmetry center of the aggregate in conformity with the normal law (4.2). In this case, ε_0 should be replaced with the mean radius R_0, while σ, with the standard deviation from the mean, σ_R. It was, however, shown (Fidder et al., 1991) that as far as the steady-state properties of the excitons are considered, the effects of random diagonal and off-diagonal disorder are almost indistinguishable. This notion in relation to the B850 excitation was confirmed in (Wu and Small, 1998). Therefore, in most of our calculations just the diagonal disorder is applied.

The disordered Frenkel exciton wavefunctions

$$|k\rangle = \sum_{n=1}^{N} a_{nk} \, |n\rangle \quad (4.3)$$

and its energy spectrum, E_k, are found by solving the eigenvalue problem

$$\sum_{m=1}^{N} \langle n| \, H_0 \, |m\rangle \, a_{mk} = \mathrm{E}_k a_{nk}. \quad (4.4)$$

The intensities and positions of the absorption bands are determined by the square of the transition dipole moments of the exciton states. The latter can be expressed as follows:

$$\mu_k = \sum_{n=1}^{N} a_{nk} \mathbf{e}_n, \quad (4.5)$$

where $\mathbf{e}_n$ stands for the unit vector of the transition dipole moment representing a Bchl molecule on site n.

Shown with the flank bold bars on Fig. 4.2a are the exciton levels calculated for a model B850 circular aggregate subject to static diagonal disorder. The foremost influence of the disorder on the exciton level structure is via spreading the state manifold (the exciton band broadening) and lifting the pair-wise degeneracy of the states. In an ensemble representation of Fig. 4.2b the Davydov bandgap is, therefore, practically lost. The underlying mechanism of these changes is the disorder-induced mixing of the Frenkel exciton eigenstates. While in a perfect aggregate the exciton wavefunctions are Bloch states spread all over the structure, in disordered aggregates they shrink and the excitons localize on smaller parts of the aggregate.[6] The mixing also relaxes

[4] The division of the static disorder into two independent types is an approximation that originates from the matrix representation of Hamiltonian (4.1). In fact, the structural and site energy disorders are interrelated.

[5] The full width at half maximum (FWHM) of the distribution function is defined as $FWHM = 2\sqrt{2\ln 2}\sigma$.

[6] In the solid-state literature, such localization is known as Anderson localization.

the strict selection rules of the regular aggregate, resulting in redistribution of the $k = \pm 1$ (and $k = \pm 8$) states transition dipole strength among other states. Hence, the lowest $k = 0$ as well as the intermediate exciton states become optically available as shown in Fig. 4.2b. Since, however, the dipole strength is still concentrated on the low-energy edge of the density of the exciton states distribution (DOS), the coherent nature of the antenna excitons is largely preserved at the moderate disorder used ($\sigma = 0.6\,V$). This justifies our usage of the same quantum number (k) entry for denoting both the delocalized excitons in regular antenna lattices as well as for the localized excitations in the disordered structures to underline their relationship.

A distribution of weak and narrow spectral holes on the low-energy side of the B850 absorption band was recorded (Reddy et al., 1992). This dispersion, conveniently named as B870, was assigned to the expected distribution of the disordered Frenkel exciton $k = 0$ states. Indeed, the individual $k = 0$ states, being the lowest excited states of the aggregate, must be spectrally very sharp. Their width at close to zero temperatures should approach $(2\pi T_1)^{-1}$, being only limited by the exciton lifetime T_1 of the order of 1–2 ns (Monshouwer et al., 1997; Timpmann et al., 2004a). The similar distribution found in LH1 was called B896 (Reddy et al., 1992). Inhomogeneous and relaxation broadening obstructs observation of the split $k = \pm 1$ (as well as of all other states) in steady-state ensemble conditions. Their presence was, however, confirmed by transient hole burning spectroscopy (Freiberg et al., 1998a, b) using spectrally narrow (transform-limited) subpicosecond laser pulses and, more directly, by single molecule fluorescence excitation spectroscopy (Van Oijen et al., 1998, 1999).

As demonstrated in Fig. 4.2b, disorder in principle opens up the whole antenna exciton band for observations by ground state absorption. The energy gap between the mean energies of the split $k = \pm 1$ and $k = \pm 8$ exciton state couples could then be operationally considered as a measure of the exciton bandwidth. In reality, however, the rather weak exciton band top (the $k = \pm 8$ states region) overlaps with broad absorbance of non-functional pigments present both in purified LH2 protein solutions as well as in intact membranes (Rätsep et al., 2005). Moreover, due to the

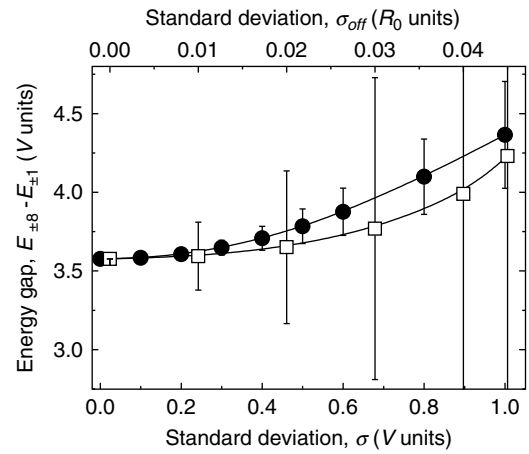

Fig. 4.3. Mean value of the energy gap between the k = ±1 and k = ±8 state couples as a function of the static disorder. The solid circles and open squares are for the diagonal and off-diagonal disorder respectively. The bars indicate standard deviation of the gap distribution functions. Off-diagonal disorder has been simulated according to reference (Jang et al., 2001) by randomly distributing the Bchl distances R_0 from the centre of the LH2 ring in accordance with normal distribution with standard deviation σ_{off}

disorder-induced band broadening (see Fig. 4.3), the very weak $k = \pm 8$ spectral structure is almost smeared out. These issues seriously complicate recording of the exciton band top using conventional absorption spectroscopy.

It turns out that boundaries of the exciton band in circular aggregates may still be accessed by taking advantage of their special polarization properties. In the regular aggregates the transition dipole moments of all degenerate state pairs are mutually perpendicular in the ring plane. We have checked that this perpendicularity is in average preserved also in the disordered aggregates with split state pairs. For each state pair then energy exists where the excitons with perpendicular polarizations will be excited at equal probability. Fluorescence anisotropy minima appear designating these excitation energies, unless the angle distribution is not too broad.

Figure 4.4 demonstrates a fairly sharp angle distribution close to the solid angle obtained for the $k = \pm 1$ states and the much broader one in case of the $k = \pm 8$ states. In agreement with experiment (Timpmann et al., 2004b, 2005), the sharp $k = \pm 1$ distribution results in deep and narrow low-energy anisotropy dip, while the broad distribution representing

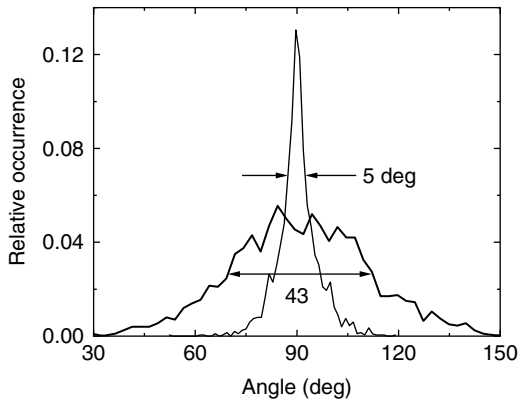

Fig. 4.4. Distributions of angles between the transition dipole moments of the k $= \pm 1$ (thin line) and k $= \pm 8$ (thick line) states calculated for an ensemble of 2000 diagonally disordered B850 aggregates with $\sigma/\mathrm{V} = 0.6$. Model parameters suitable for the LH2 from *Rps. acidophila* have been used. Indicated are FWHMs of the distribution functions

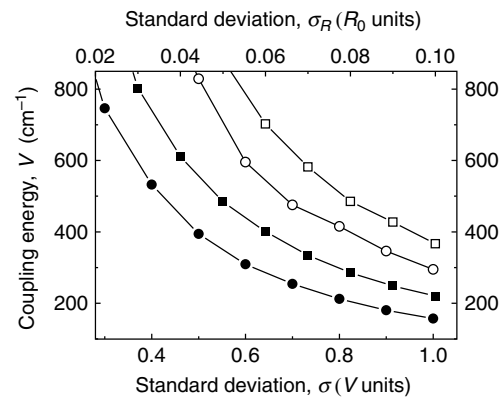

Fig. 4.5. Consistency plots for the diagonal (circles) and off-diagonal (squares) disorder models of the LH2 excitonic states. The open symbols correspond to the average gap between the $k = 0$ state energy and the midpoint of the $k = \pm 1$ state energies. Solid symbols represent the FWHM of the $k = 0$ state energy distribution

the $k = \pm 8$ states produces but a shallow high-energy anisotropy depression. Since the remaining state pairs confirmed still larger average deviation from the solid angle than the $k = \pm 8$ states, the anisotropy minima are practically observable only for the $k = \pm 1$ and $k = \pm 8$ exciton band border states (see further details in Section V). Given that off-diagonal disorder creates more diffuse band edges than diagonal disorder (see Fig. 4.3), the latter model is better suited for description of the antenna fluorescence anisotropy data (Trinkunas and Freiberg, 2006).

III. Shortcomings of the Disordered Frenkel Exciton Model

We have already pointed out that the B870 zero-phonon hole distribution was interpreted as a distribution of the lowest ($k = 0$) states of the Frenkel excitons in disordered ensembles of the B850 aggregates. Yet, calculations have shown (Freiberg et al., 1999, 2003b) that if the exciton coupling energy and the standard deviation of the disorder are kept within the commonly accepted limits, it is impossible to reproduce the B870 band in terms of its width, relative peak position (with respect to the B850 absorption maximum, ΔE), and fractional intensity (relative to the total B850 absorption intensity). Figure 4.5 highlights the same inconsistency from a different prospective.

The FWHM and ΔE both depend on disorder as well as on exciton coupling energy. Therefore, it is possible to build two separate curves (one for FWHM and the second for ΔE) that describe the relationship between the coupling energy and the disorder by fixing each parameter to its experimental value (FWHM $= 147\,\mathrm{cm}^{-1}$ and $\Delta E = 204\,\mathrm{cm}^{-1}$, as measured for the LH2 complexes from *Rb. sphaeroides* at 5 K (Freiberg et al., 2003b; Timpmann et al., 2004a)). A crossing of the curves would then provide consistent values of the coupling energy and disorder variables. As can be seen from Fig. 4.5, no crossing is observed within realistic limits of the coupling energy (V between 100 and $1{,}000\,\mathrm{cm}^{-1}$) and relative disorder (σ/V between 0.2 and 1.0 or σ_R/R_0 between 0.02 and 0.1).

Listed below are a few other experimental observations for ensembles of LH2 complexes that cannot find satisfactory explanation within the disordered Frenkel exciton approach:

(i) Due to weak exciton–phonon coupling suggested by the hole burning experiment (Reddy et al., 1992), the resonant fluorescence spectrum cannot be much broader than the B870 absorption band. However, the width of the respective ensemble emission spectrum exceeds this figure by more than a factor of two (Freiberg et al., 1999, 2003b).

(ii) Evidence has been found from the FLN experiment that the broad emission spectrum is essentially homogeneously broadened suggesting that the exciton–phonon coupling for the transition from the relaxed excited state must be strong (Timpmann et al., 2001). This is in contrast with the red edge of the absorption spectrum, which appears mostly inhomogeneously broadened. For LH1 complexes, similar inconsistencies between the narrow hole burning absorption spectra (Reddy et al., 1992) and broad FLN spectra (Van Mourik et al., 1992; Monshouwer et al., 1995; Timpmann et al., 2004a) have been noticed and discussed (Pullerits et al., 1994; Timpmann et al., 2004a).

(iii) Rising the temperature from cryogenic temperatures to room temperature should thermally populate the strongly allowed $k = \pm 1$ exciton states and result in a significant reduction of the fluorescence lifetime. Yet, the fluorescence lifetime is virtually independent on temperature up to $\sim$170 K, while shortening thereafter only by about 20% (Freiberg et al., 2003b). On the basis of the exciton model this can only be explained by assuming static disorder that is much too large to be consistent with the absorption spectrum.

(iv) To explain temperature dependences of the conjugate absorption and fluorescence spectra of LH2 complexes from three different bacterial species using the same dynamic theory model an extra red shift of the lowest exciton state by $\sim$90 cm^{-1} was required (Urboniene et al., 2005, 2007).

It is thus quite clear that the genuine Frenkel exciton model, which includes only static disorder, misses some essential aspects of the reality. In solids the phonons scatter the excitons causing homogeneous line broadening (Mukamel, 1995). Strong scattering also leads to fast processes on time scales of the nuclear movements known as excitonic polaron formation and exciton self-trapping. The latter term refers to the fact that by coupling to the surroundings the exciton may induce a deformation of the lattice that lowers the exciton energy and causes its long-time trapping on a limited region of the material space (Lu and Mukamel, 1991; Meier et al., 1997; Tanaka, 2003). In bulk ionic and molecular crystals, where the exciton self-trapping is most thoroughly studied (Rashba, 1982; Ueta et al., 1986; Song and Williams, 1992), characteristic multi-phonon self-trapped exciton emission bands are commonly observed. These broad and featureless spectra are much red shifted (Stokes shifted) relative to the typically more structured free exciton emission bands.

One could think of the B850 and B875 circles of resonantly coupled Bchl molecules as being electronically one-dimensional (1D). This concept is valid as long as the nearest-neighbor couplings much surpass those between the non-nearest-neighbors and also the symmetry-breaking electron-lattice couplings. Differently from regular two-dimensional (2D) and three-dimensional (3D) lattices, where self-trapping has an energetic threshold and happens abruptly, in 1D arrays the process is smooth taking place at any non-vanishing electron-lattice coupling energy (Rashba, 1982; Sumi, 1994; Cruzeiro-Hansson et al., 2000). Similar topological differences exist relative to the Anderson localization. Therefore, in contrast to the bulk solids, the spectra of the excitons self-trapped in 1D lattice may necessarily not be broad and a great deal Stokes shifted. Clear-cut spectra corresponding to shallow self-trapped excitons have been recorded in some low-symmetry molecular crystals such as β-perylene (Matsui et al., 1984). As follows, a polaronic model of excitons in the B850 and B875 antenna aggregates is introduced. The model is based on the adiabatic Holstein Hamiltonian (Holstein, 1959), being the simplest means to introduce polaronic effects into 1D molecular arrays. Alternative approaches, which, however, have not been applied for comparison with experiment, can also be found (Meier et al., 1997; Damjanovic et al., 2002).

IV. Excitonic Polaron Model of the Antenna Fluorescing States

The relevant excitonic polaron Hamiltonian reads:

$$H = H_0 + c \sum_n q_n |n\rangle\langle n| + \frac{1}{2} \sum_n q_n^2. \quad (4.6)$$

It is modified compared with the original Holstein equation by including static disorder in the rigid-lattice Hamiltonian, H_0, as shown in Eq. (4.1). The second term in Eq. (4.6) stands for the exciton–phonon coupling energy and the

last term represents the lattice potential energy. The lattice kinetic energy is ignored because of the applied adiabatic approximation, $\nu_m / V \ll 1$, where ν_m is the vibrational frequency inducing the polaronic lattice distortion. Further variables in Eq. (4.6) are q_n, the local lattice distortion at site n and c, the coupling constant characterizing the short-range, on-site exciton–phonon coupling. It is worth noticing here that $c^2/2 = E_{LR}$ defines the site reorganization energy, i.e. an energy which is thermalized (absorbed by the surrounding lattice) as a result of optical excitation/excited state decay in a single antenna site.

By expressing the eigenstates of the exciton–lattice system in the basis of local state vectors

$$|v\rangle = \sum_n \varphi_{nv} |n\rangle \tag{4.7}$$

with amplitudes φ_{nv}, the expectation value of the Hamiltonian (4.6) can be derived as:

$$\begin{aligned} J_v(\{\varphi_{nv}\}, \{q_n\}) = \langle v| H |v\rangle &= \sum_n \varepsilon_n \varphi_{nv}^* \varphi_{nv} \\ &+ \sum_n \sum_{m(\neq n)} t_{nm} \varphi_{nv}^* \varphi_{mv} \\ &+ c \sum_n q_n \varphi_{nv}^* \varphi_{nv} \\ &+ \frac{1}{2} \sum_n q_n^2 \Big(\sum_m \varphi_{mv}^* \varphi_{mv} \Big). \end{aligned} \tag{4.8}$$

Population of the quantum states is defined by temperature. In case of sparse states and at sufficiently low temperatures, the conditions that are relevant to our subjects, only the lowest-energy or ground excitonic polaron state is populated. Normalization of the ground state (indicated by subscript 0) amplitudes of the excitonic polarons, φ_{n0}, is accomplished by adding a Lagrange multiplier E_0:

$$J_0' = J_0 - E_0 \Big(\sum_i \varphi_{i0}^* \varphi_{i0} - 1 \Big). \tag{4.9}$$

To determine the ground state properties, such as its energy, localization length, and reorganization energy, variations of the functional (4.9) with respect to parameters $\{\varphi_{n0}\}$, $\{q_n\}$, and E_0 are performed. By varying $\{\varphi_{n0}^*\}$, a system of coupled equations is obtained

$$\left[\varepsilon_n + cq_n + \frac{1}{2} \left(\sum_i q_i^2 \right) \right] \varphi_{n0} + \sum_{m(\neq n)} t_{nm} \varphi_{m0} = E_0 \varphi_{n0}, \tag{4.10}$$

where the optimal distortions,

$$q_n = - \frac{c \varphi_{n0}^* \varphi_{n0}}{\sum_i \varphi_{i0}^* \varphi_{i0}}, \tag{4.11}$$

have been found from the following condition:

$$\frac{\partial J_0'(\{\varphi_{n0}\}, \{q_n\})}{\partial q_n} = 0. \tag{4.12}$$

The optimal distortions obey a sum rule

$$\sum_n q_n = -c. \tag{4.13}$$

By substitution the distortions (4.11) into Eq. (4.10) a coupled system of discrete nonlinear Schrödinger equations is obtained for the optimal ground-state exciton amplitudes

$$\varepsilon_n \varphi_{n0} + \sum_{m(\neq n)} t_{nm} \varphi_{m0} - c^2 |\varphi_{n0}|^2 \varphi_{n0} = E_0 \varphi_{n0}. \tag{4.14}$$

These amplitudes determine the modified potential of the site energies due to dynamic lattice deformations:

$$\tilde{\varepsilon}_n = \varepsilon_n - \frac{c^2}{2} |\varphi_{n0}|^2. \tag{4.15}$$

Equations (4.14) are nonlinear with respect to the amplitudes φ_{n0}. The cubic term, proportional to c^2, while introducing dependence of the ground state properties on initial excitation amplitudes, also excludes analytic solutions of Eq. (4.14), even for the simplest set of the coupling matrix elements. This problem was overcome by applying an iterative procedure described in (Noba and Kayanuma, 1998). In this method, the distortions (4.11) are first calculated for certain initial or seed (hence the superscript s) set of amplitudes, $\{a_{nk}^s\}$. Then, Eq. (4.10) are solved numerically using distortions as parameters. The obtained lowest state eigenvector is subsequently used as a seed for the next iteration. The procedure is repeated until convergent energy and amplitudes are obtained.

A. Ground States of the Excitonic Polarons in Regular and Disordered Circular Aggregates

The most important parameters characterizing excitonic polarons and/or self-trapped excitons in the ground state are their energy, E_0^s, localization length (or shortly size), L_0^s, and superradiance enhancement factor, F_0^s.

The eigenvalue E_0^s is obtained as an expectation value of Hamiltonian (4.6), $E_0^s = min\ J_v(\{\varphi_{n0}^s\})$. In experimental spectra, it relates to sharp zero phonon lines (ZPL), representing the phononless energy of self-trapped excitons. The phonon sidebands (PSB) that accompany ZPLs in absorption/fluorescence spectra lay above/below the ZPL energy. Their maxima are shifted relative to the ZPL position by a potential energy of lattice distortion, λ_0^s, also called reorganization energy:

$$\lambda_0^s = \frac{c^2}{2} \sum_n |\varphi_{n0}|^4. \tag{4.16}$$

The localization length, L_0^s, may be defined as the inverse participation ratio (Leggett et al., 1987; Fidder et al., 1991; see Dahlbom et al., 2001 for other conventions) that represents the size in terms of the lattice sites shared by the excitonic polaron wavefunction:

$$L_0^s = \frac{1}{\sum_n |\varphi_{n0}|^4}. \tag{4.17}$$

From Eqs. (4.16) and (4.17) it then appears that the reorganization energy is inversely proportional to the excitonic polaron size:

$$\lambda_0^s = \frac{c^2}{2L_0^s}. \tag{4.18}$$

The superradiance enhancement factor, F_0^s, measures emission intensity of excitonic polarons relative to that of single solvated pigments:

$$F_0^s = \sum_{nm} (\mathbf{e}_n \mathbf{e}_m)\, \varphi_{n0}^* \varphi_{m0}. \tag{4.19}$$

Polaronic features of excitons depend most on the dimensionless coupling constant, g, being defined as a ratio, $g = E_{LR}/2V = c^2/4V$, of the site reorganization energy and half of the exciton bandwidth. When g exceeds a certain threshold value, g_c, the excitons in 2D and 3D systems abruptly self-trap. At $g > g_c$, both delocalized (free) and localized (self-trapped) excitons may coexist, separated by a potential barrier in a configurational coordinate space. In ordered 1D systems, however, just a single ground state is present. Its properties change smoothly with g beginning from a totally delocalized exciton state at $g = 0$ towards progressively more localized (self-trapped) states (Rashba, 1982; Kabanov and Mashtakov, 1993; Sumi, 1994; Noba and Kayanuma, 1998; Romero et al., 1999).

Disorder breaks ideal periodicity of the circular antenna aggregates. Therefore, all their states are more or less Anderson-localized from the outset, i.e., already at $g = 0$. The concrete state properties are, however, determined by a combined effect of the resonant interaction, static disorder, and exciton–phonon coupling. In that the latter factor may be decisive. It has been shown (Trinkunas and Freiberg, 2005) that in disordered 1D aggregates the exciton–phonon coupling not only promotes further localization of excitons (beyond the margin set by competition of resonant interaction and static disorder) but, similar to the 2D and 3D lattices, it also introduces abrupt self-trapping type branching of the states at certain critical g value. These branched states can be obtained by solving Eq. (4.10) for two seed amplitude distributions, one that corresponds to a localized single-site excitation and the second, to a totally delocalized excitation creating equal amplitudes on all sites. Multiple stable self-trapped excitons with different size and reorganization energy may thus coexist in a disordered 1D array if exciton–phonon coupling is sufficiently strong.

Figure 4.6 presents the ground state characteristics (E_0^k, L_0^k, and F_0^k) of excitonic polarons in a single diagonally disordered B850 aggregate as a function of g. The simulations are performed for the initial amplitude distributions that correspond to the first three ($k = 0, \pm 1$) disordered Frenkel exciton eigenvectors (Eq. 4.3). The seed amplitude distributions with equal (delocalized) or single-site (localized) excitation probabilities referred to above have no practical reasoning because it is hard to produce such initial states. At the same time, it is in principle possible to selectively excite the disordered Frenkel exciton

states using narrowband lasers. The only limitation is that the energy gap between the adjacent exciton states in the rigid lattice should be larger than the characteristic phonon energy, $h\nu_m$, mixing these states. We shall revisit this issue in Section V.B.

As can be seen from Fig. 4.6, by exciting the $k = 0$ state all the three characteristics follow a smooth path with increasing g, typical for the regular 1D aggregate. Yet, the self-trapping transition that in this particular case is recognizable at $g \approx 0.55$ by contraction of the excitonic polaron size (panel b) as well as by strong increase of its emission strength (panel c) generally appears much earlier than in the ordered aggregate (see Fig. 4.8 below). The dependences for $k \neq 0$ seed distributions are even more intricate. They initially follow the same path as the $k = 0$ state but then new branches split off (at the g values indicated with vertical dashed lines). All the three initial conditions thus result in self-trapped excitons, which have distinct ground state energies as well as other characteristics. Different states on one and the same aggregate can be stable only if they are separated by energy barrier(s). Energy transfer along such a structure is enabled by incoherent hopping mechanism or by tunneling, the former mechanism being temperature-sensitive, while the latter not.

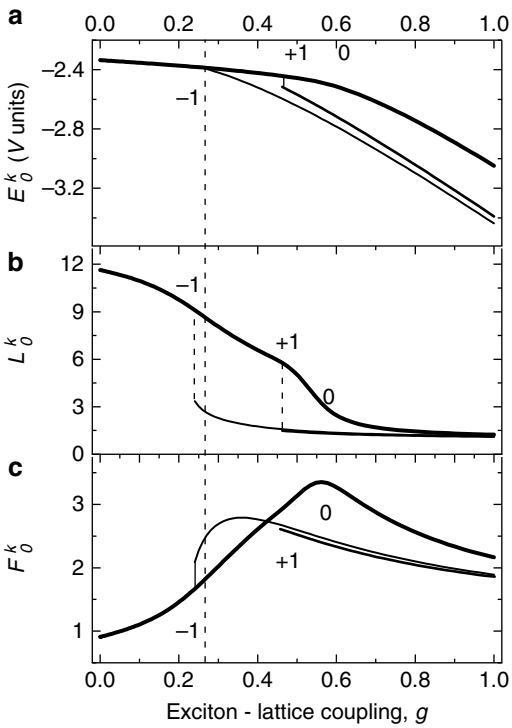

Fig. 4.6. Ground state properties – (**a**), the energy, (**b**), the localization length and (**c**), the superradiance enhancement factor – of the three excitonic polaron states distinguished by the initial amplitude distributions k in diagonally disordered circular aggregates as a function of the exciton-lattice coupling constant g. A single realization of diagonally disordered site energies as shown in Fig. 4.7b is applied to calculate the data. Dashed vertical lines indicate abrupt changes (bifurcations) of the state properties discussed in the text. The vertical dotted line at $g = 0.27$ crossing all panels points the coupling strength used when calculating the distributions of the lattice deformation energy in Fig. 4.7a

To visualize conformational distortions of large cyclic aggregates such as B850 caused by dynamic exciton–phonon coupling, it is helpful to stretch out the molecular subunits in a linear way and plot the deviations from the site energies according to Eq. (4.15) against the site number. Figure 4.7a presents such distributions for the two self-trapped exciton states of Fig. 4.6, simultaneously supported at $g = 0.27$. The respective static site energy distribution is shown in Fig. 4.7b. One can observe that the deformations corresponding to the two states are largely localized on separate areas of the aggregate. Also, excitons tend to self-trap around the sites with lowest energy, in agreement with (Emin and Bussac, 1994; Stoneham et al., 2007).

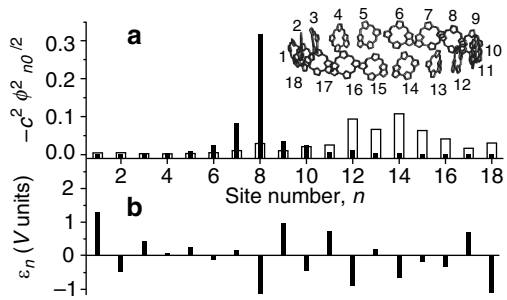

Fig. 4.7. Distributions of the lattice deformation energy due to dynamic exciton–phonon coupling (Eq. 4.15) (**a**) and the corresponding distribution of static site excitation energies (**b**). The linear string of the lattice sites numbered from 1 to 18 schematically represents the circular aggregate shown in the insert. The solid and empty bars in (a) correspond to the two self-trapped exciton states in Fig. 4.6 that are supported in the same disordered B850 aggregate at $g = 0.27$, labeled with $k = 0$ and $k = -1$, respectively

B. Ensemble-averaged Characteristics of the Antenna Excitonic Polarons

The data in Figs. 4.6 and 4.7 represent just a single diagonal disorder realization sampled out from the distribution (4.2) of molecular rings that are assumed to simulate the B850 antenna complexes. We are already aware that the onset of self-trapping and the number of coexisting states depend on excitation. In statistical ensembles of antenna rings the excitation conditions vary considerably from ring to ring due to fluctuating absorption spectra. Figure 4.8 provides ensemble characteristics of the excitonic polarons in the B850 antenna aggregates as a function of g, averaged over 5,000 diagonal disorder realizations.

As one can see, within the wide error bars the overall behavior of the curves in Fig. 4.8 is similar for those in Fig. 4.6. The large uncertainty is due to disorder and varying excitation conditions as emphasized above. With growing exciton–phonon coupling the excitonic polaron energy and its localization length both smoothly decrease beginning from the respective average disordered Frenkel exciton values of $-2.5\,V$ and of 6.3 sites. At the selected relative static disorder $\sigma = 0.6\,V$, which satisfies most of the experiments, see Section V), the Frenkel excitons are localized on about one third of the aggregate circle. Dynamic interactions further reduce this size. At $g \approx 0.3$, relevant for the LH2 complexes, the average number of occupied sites is just 3.1, more than twice less compared with the initial ($g = 0$) value. The behavior of F_0 is most fascinating (Fig. 4.8c). The relative emission power, being initially as high as 2.1 grows with g, achieves a maximum of $\sim$3.0 at $g \approx 0.3$, and decreases thereafter. The efficiency of incoherent excitation energy transfer increases with emission rate of the donor molecules (Scholes, 2003). Any process that enhances the antenna ability to emit thus serves for optimization of photosynthetic energy transfer and trapping processes. The inset on Fig. 4.8c compares distributions of superradiance enhancement factors at $g = 0$ and 0.3. It is obvious that in the LH2 complexes the efficiency gain due to exciton self-trapping may be essential. Due to different geometry, however, the increase of F_0 in LH1 is rather minor (from five to less than six).

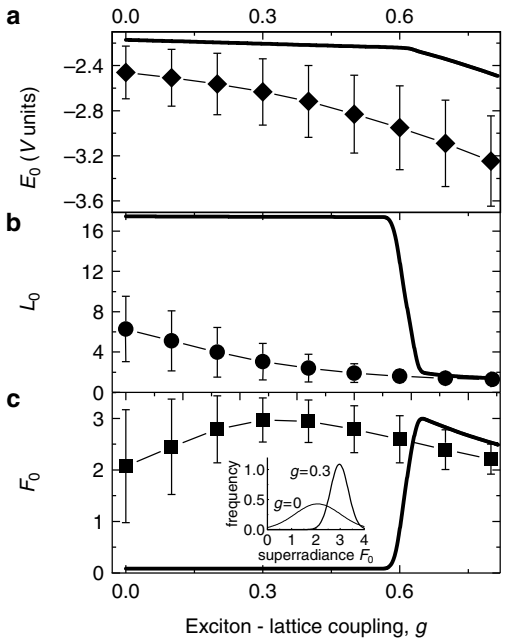

Fig. 4.8. Ensemble averaged characteristics of self-trapped excitons in the B850 aggregates as a function of the exciton-lattice coupling constant: (**a**) energy; (**b**) localization length and (**c**) superradiance enhancement factor. Average is taken over 5,000 samples from the Gaussian distribution (Eq. 4.2) with $\sigma = 0.6\,V$ and $\varepsilon_0 = 0$. The symbols and error bars designate the mean and the FWHM, respectively, of the corresponding distributions. The inset on panel c shows the normalized distribution of superradiance enhancement factors at $g = 0$ and at $g = 0.3$. Shown with thick solid line are the data for the regular (disorder free) B850 aggregate

The large effects of disorder on the excitonic polaron characteristics may be best appreciated from comparison with the regular circular aggregate (bold curves in Fig. 4.8). As it was already noticed, disorder considerably reduces the exciton–lattice coupling strength required for the exciton self-trapping. While in the regular B850 aggregate the self-trapping transition is expected at $g = 0.6$, in qualitative agreement with previous works on linear aggregates (Kabanov and Mashtakov, 1993; Sumi, 1994; Noba and Kayanuma, 1998), it occurs at $g \approx 0.3$ in more realistic disordered conditions. Other effects of disorder apparent in Fig. 4.8 (lowering of the transition energy, shrinking of the exciton size, and redistribution of the dipole strength between the exciton states) have been discussed in Section II and do not require further comments.

A well-known qualitative relationship exists between the free exciton size and its transition

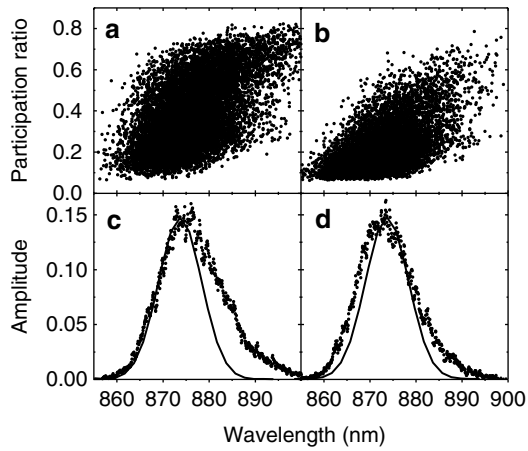

Fig. 4.9. (**a**) Relationship between the participation ratio L_0^{-1} and the ZPL position chE_0^{-1} for the ground state of self-trapped excitons at $g = 0.24$. (**b**) The same as in panel (**a**) for the lowest $k = 0$ Frenkel exciton states ($g = 0$). Panels (**c**) and (**d**), the distribution of zero-phonon holes (the B870 band) for the B850 aggregates in B800 deficient LH2 complexes from *Rb. sphaeroides* (solid lines) and the simulated distributions of the relative transition dipole strength for the two models (scattered points). A diagonally disordered ensemble of 10^4 aggregates emulating B800 deficient LH2 complexes has been used in the simulations

energy: the larger the exciton, the lower its energy (Scholes and Rumbles, 2006). Here, we are trying to establish whether similar correlation exists in disordered ensembles of self-trapped (Fig. 4.9a) and Frenkel (Fig. 4.9b) excitons. For convenience the data in Fig. 4.9 are plotted in the $L_0^{-1} - chE_0^{-1}$ (exciton participation ratio – wavelength of ZPL) axes scale. Here h and c have the usual meaning of the Planck's constant and of the speed of light, respectively. An ensemble of the B800 deficient LH2 complexes was assumed characterized with $g = 0.24$. At this exciton–lattice coupling constant the majority of the antenna rings host just a single self-trapped exciton state, while about 10% of them support two such states.

Figures 4.9a and b illustrate positive correlations that exist between the participation ratio and the ZPL position in the ensembles of self-trapped excitons and excitons, respectively. The excitons and self-trapped excitons that absorb/emit at longer wavelengths are generally more localized. However, the slope of an imaginary line through constellations of the data points is considerably greater in the case of the self-trapped excitons than excitons. Furthermore, while the Frenkel exciton data points are densely flocking on the low left hand corner of the graph signifying delocalization, the data for the self-trapped excitons are widely spread toward more localized states.

Figures 4.9c and d compare the calculated according to Eq. (4.19) distributions of the relative transition dipole strength with the experimental distribution (Freiberg et al., 2003b; Rätsep et al., 2005) of zero-phonon holes (the B870 band). As seen, the excitonic polaron model (Fig. 4.9c) is able to reproduce the high-energy slope and the maximum of the experimental curve very well. The discrepancy observed at the low-energy side is explained by the fact that the simplified calculations do not take into account the actual spectral lineshapes. As it will be in more detail described below, the transition dipole strength in the excitonic polaron spectra is shared by narrow ZPL and broad PSB. Division of intensity between these components depends on size of the excitonic polarons. At blue side intense ZPLs dominate the spectrum, whereas at red side the spectral intensity is concentrated into PSBs. By virtue of the hole burning technique, the low-burn distribution of the zero phonon hole depths (the B870 band) emphasizes contribution of the ZPLs. In agreement with Fig. 4.9c, therefore, a decent fit could only be expected at high-energy side of the spectrum where most exciton-like excitonic polaron states donate. The match in the case of the Frenkel exciton model (Fig. 4.9d) is in almost every aspect much less satisfactory.

At any excitation wavelength the antenna rings corresponding to broad range of participation ratios and, according to Eq. (4.18), of reorganization energies are simultaneously excited. Since the reorganization energy is related to the shift and broadening of the spectra, the efficiency of selective spectroscopy methods (such as hole burning and FLN) is reduced when applied to ensembles of self-trapped excitons. Let us explain the situation once again using a configuration coordinate representation of Fig. 4.10.

The four excited state parabolas in this figure represent two free exciton states (with their potential energy minima unshifted relative to the ground state curve) and two self-trapped exciton

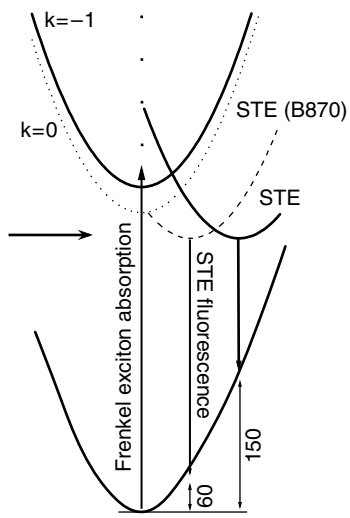

Fig. 4.10. A configuration coordinate diagram for excitations in B850 antenna aggregates. The shifted self-trapped exciton (STE) diabatic potential energy curves are for the two self-trapped exciton states (represented by dashed and thick solid lines) that belong to different or the same antenna rings. The numbers denote approximate reorganization energies in wave numbers estimated from the selective fluorescence data for the B850 aggregates from *Rb. sphaeroides*. The un-shifted excited states indicated with k-numbers represent average positions of the two lowest disordered exciton distributions in Fig. 4.2b

states (shifted curves).[7] The self-trapped excitons selected out from an ensemble of the B850 rings have the same ZPL energy but different reorganization energies (small for dashed and large for thick solid line). Therefore, the fluorescence recorded upon resonant excitation with a narrowband laser (horizontal arrow) appears to be a sum of two (narrow for small and broad for large reorganization energy) overlapping spectra that are difficult to separate. No such broadening mechanism is available for the Frenkel excitons. At all excitation wavelengths nearly the same sharp lineshape is produced. Obviously, only the excitonic polaron model is compatible with the experiments on LH2 and LH1 antenna complexes where poor selectivity of the FLN spectra was observed (Van Mourik et al., 1992; Freiberg et al., 2003a, b; Monshouwer et al., 1995).

[7] An energy difference between the $k = 0$ exciton state and the self-trapped exciton states is due to dynamic lattice deformation. Therefore, by analogy with regular lattices, it might be called the self-trapping binding energy.

V. Evaluation of the Model Parameters from the Experimental Spectra

A. Resonant Coupling Energy, Inhomogeneous Spectral Broadening, and Reorganization Energy

The excitonic polaron model identifies three main parameters that determine the true nature of the photosynthetic antenna excitations, those being the resonant (exciton) coupling energy, the inhomogeneous spectral broadening, and the reorganization energy. Large amount of heterogeneity usually prevents assessment of these parameters from the conventional optical spectra of aggregates. Non-conventional approaches are, therefore, required to obtain necessary information and to test the models. As follows, a method of evaluation of the interrelated exciton coupling energy, inhomogeneous spectral broadening, and reorganization energy from fluorescence anisotropy spectra is demonstrated (Timpmann et al., 2004a, 2005; Trinkunas and Freiberg, 2006).

Figure 4.11 shows fluorescence anisotropy as a function of the linearly polarized excitation light wavelength for the B800-deficient LH2 complexes from *Rb. sphaeroides*. This mutant sample was chosen for the illustration in order to display the B850 spectroscopy in its most basic form, having getting rid from the complications due to the quasi-monomeric B800 molecules.

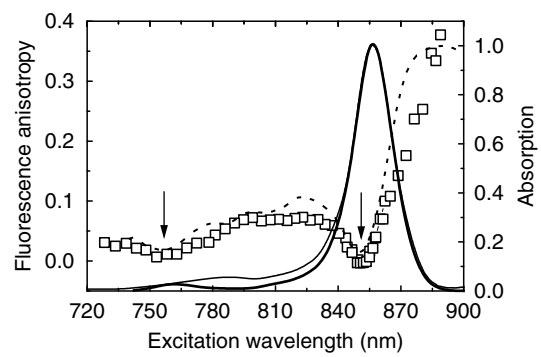

Fig. 4.11. Absorption (measured: thin solid curve; simulated: thick solid curve) and fluorescence anisotropy (see Eq. 4.23) excitation spectra (experimental: squares; simulated: dashed curve) of purified B800-deficient LH2 complexes from *Rb. sphaeroides* at 5 K. The polarized fluorescence was recorded broadband at the long-wavelength part of the emission spectrum where the anisotropy is constant

The fluorescence anisotropy, r, is related to the linearly polarized fluorescence emission intensities I_{vv} and I_{vh} as

$$r = \frac{I_{vv} - I_{vh}}{I_{vv} + 2I_{vh}}. \tag{4.20}$$

Here, the I_{vv} and I_{vh} are the emission intensities polarized, respectively, parallel and perpendicular to the orientation of the electric vector of the excitation light. In agreement with the previous measurements on wild type complexes (Kramer et al., 1984; Visschers et al., 1995; Timpmann et al., 2004b), the low anisotropy observed at shorter wavelengths rises steeply across the B850 absorption band closing a theoretical limit of 0.4 at its long-wavelength slope. In addition, however, there are two anisotropy drops pointed out with arrows, a shallow high-energy depression at 757 nm and a deeper and narrower low-energy dip at 851 nm. As discussed above, these minima could be related to the weakly ($k = \pm 8$) and strongly ($k = \pm 1$) absorbing exciton band edges, respectively.

The fluorescence spectrum (with emission frequency ν_e) of a single LH2 complex upon selective excitation at ν_a can be calculated as (Trinkunas and Freiberg, 2006):

$$I(\nu_e, \nu_a) = N_{pol}^{-1} \sum_k \left|\mu_k\right|^2 \left|\mu^k\right|^2 F^k(\nu_e) \times \int_{-\Delta/2}^{\Delta/2} A(E_k - \nu_a + \nu') d\nu'. \tag{4.21}$$

In Eq. (4.21), μ_k is the transition dipole moment vector of the absorbing Frenkel exciton states (Eq. 4.5), μ^k is the transition dipole moment vector of the emitting excitonic polaron states, $F^k(\nu_e)$ is the normalized emission profile of self-trapped excitons, $A(E_k - \nu_a)$ is the normalized homogenously broadened absorption profile of Frenkel excitons centered at E_k, and N_{pol} is the number of different self-trapped exciton states per complex. At low temperatures when energy transfer is absent the fluorescence from all these states should be accounted for independently. The sum in Eq. (4.21) counts the Frenkel exciton states that have energy between $\nu_a - \Delta/2$ and $\nu_a + \Delta/2$ and is required for comparison with experiment, because Δ limits the available excitation selectivity (Agarwal et al., 2002; Freiberg et al., 1999). $\Delta = \sqrt{8 \ln 2}\sigma_{ext}$, where σ_{ext}, the standard deviation of the external diagonal disorder, is determined by random variations of the mean transition energy in different complexes.

The emission profile, $F^k(\nu_e)$, is modeled by a function:

$$F^k(\nu_e) = l(E_0^k) \exp\left(-\frac{\lambda_0^k}{h\nu_m}\right) + f^k(\nu_e)\left[1 - \exp\left(-\frac{\lambda_0^k}{h\nu_m}\right)\right], \tag{4.22}$$

where $l(E_0^k)$ represents the ZPL centered at E_0^k and $f^k(\nu_e)$, the associated PSB. The dimensionless parameter $S = \lambda_0^k / h\nu_m$, commonly named as the Huang-Rhys factor, corresponds to an average number of phonons that accompany absorption or fluorescence emission transitions (see, e.g., Rebane, 1970). In actual computations that assumed extreme low temperatures, the shape of $l(E_0^k)$ was approximated by a Gaussian of experimentally limited FWHM ($\sim 1.5\,\mathrm{cm}^{-1}$), while that of $f^k(\nu_e)$, by the following function:

$$f^k(\nu_e) = \begin{cases} \frac{E_0^k - h\nu_e}{(\lambda_0^k)^2} \exp\left(-\frac{\left|E_0^k - h\nu_e\right|}{\lambda_0^k}\right), & h\nu_e < E_0^k \\ 0, & h\nu_e \geq E_0^k \end{cases}. \tag{4.23}$$

The fluorescence anisotropy dependence for a single aggregate was computed using an equation $r_k = (3\cos^2\alpha_k - 1)/5$ (α_k is the angle between the transition dipole moment vectors of absorbing (μ_k) and emitting (μ^k) states). At low temperatures the emitting state is always the ground state of the self-trapped excitons. The parallel, I_{par}, and perpendicular, I_{per}, fluorescence emission components were obtained from Eq. (4.21) by multiplying each k-term under the sum with orientation factors $1 + 2r_k$ and $1 - r_k$, respectively. Ensembles averages $< I_{par} >$ and $< I_{per} >$ were then calculated, being directly related to the experimental intensities I_{vv} and I_{vh}, respectively.

The simulated data, averaged over an ensemble of 10,000 diagonal disorder realizations, are compared with the experiment in Fig. 4.11. The couplings between all pigment were calculated in transition dipole–dipole approximation using the crystallographic structure of LH2 of *Rps. acidophila* strain 10,050 (Papiz et al., 2003). Adjusted by fitting circular dichroism spectra, the site energy difference in the basic heterodimer unit was set to a value of $0.8\,V$. Similar figure was suggested by (Koolhaas et al., 1997). Simultaneous fine-tuning of this number of free parameters for large ensembles is computationally costly. To curtail the procedure, an iterative approach briefly described below was applied. We began with simulations of the absorption spectrum, from which rough estimates for the relative disorders, σ/V and σ_{ext}/V were obtained. Then a zero-order value of V was evaluated from simulations of the anisotropy curve. Finally, the fluorescence spectrum characteristics (peak position and FWHM) were fitted as a function of excitation wavelength. This comparison is sensitive to the site reorganization energy, E_{LR}, as well as to the mean vibrational frequency, ν_m. The emission bandshape is also susceptible to disorder. Adjustment of the disorder parameters for the emission spectrum launched next twist of the search. The iterative procedure was continued until satisfactory match with experimental data was achieved.

The fits in Fig. 4.11 seem very reasonable, considering the possibility that slight differences between real and used crystal structures may exist. Moreover, the calculated spectra understandably lack any contribution from the nonfunctional Bchls (see Rätsep et al., 2005). This in large explains the absorption spectrum discrepancy observable at 787 nm. The anisotropy curve very well reproduces the positions of the two experimental minima. The deviations observed in the middle and upper exciton band regions with higher DOS (see Fig. 4.2b) may be explained by partial failure of the adiabatic criterion in this range. Comparison with the absorption spectrum proves that the two anisotropy minima are indeed well correlated with the $k = \pm 1$ and $k = \pm 8$ states at the exciton band boundaries. The best-fit parameters obtained from all these comparisons are gathered into Table 4.1. For overview, Table 4.1 also includes fitting parameters for all other bacterial antenna aggregates analyzed so far with similar approach. Due to space limits, however, we cannot comment on those other results in any length.

B. The Wavelength-dependent Exciton–Phonon Coupling and the Weighted Density of the Phonon States

Much of the controversy underscored in Section III between the absorbing and emitting properties of the LH2 and LH1 antennas is a result of the early estimates (Reddy et al., 1992; Wu et al., 1997a) of the Huang-Rhys factor and the effective phonon frequency: $S \approx 0.3$ and $V_m \approx 20\,\mathrm{cm}^{-1}$, respectively. These numbers, obtained from the photophysical hole-burning experiments, suggest very small reorganization energy compatible with rather weak exciton–phonon coupling. It was only recently realized (Pieper et al., 1999; Rätsep and Freiberg, 2003) that the hole-burning spectra of the antenna complexes are strongly distorted due to limited inhomogeneous spread of the lowest

Table 4.1. Model parameters for the B820, B850, and B875 ring aggregates of bacterial antenna complexes[a]

Sample	V/V' cm^{-1}	$\sigma_{\mathrm{int}}/\sigma_{ext}$ cm^{-1}	$\langle\varepsilon_0\rangle_{ext}$ cm^{-1}	E_{LR} cm^{-1}	g	$\frac{\sigma_{\mathrm{int}}}{V}$	Bandwidth[b] (sim/exp)
LH2 from *Rb. spaeroides*	315/245	220/60	12,390	160	0.25	0.70	1,280/1,250
B800-deficient mutant LH2 from *Rb. spaeroides*	370/290	240/60	12,400	190	0.26	0.65	1,450/1,500
LH2 from *Rps. acidophila*	350/270	180/40	12,160	200	0.28	0.51	1,480/1,450
LH3 from *Rps. acidophila*	320/250	200/50	12,800	180	0.28	0.64	1,300/1,290
LH1 from *Rb. spaeroides*[c]	420/330	230/50	12,130	185	0.22	0.55	1,950/1,950

[a]The estimated standard deviation of the parameters is typically 10%, except for the mean of the Bchl transition energies $\langle\varepsilon_0\rangle_{ext}$ where it is about 0.25%.
[b]Exciton bandwidth determined as an energy gap between the anisotropy dips (sim: from simulations, exp: from experiments).
[c]Apparent variances with the data in (Timpmann et al., 2004a) are explained with different static disorder models applied.

states. Moreover, since the photophysical bleaching mechanism just redistributes the hole burning products within the spectra range of the original absorption band, the hole burning spectra are obscured by the absorbance of the products. A thorough analysis made in (Rätsep and Freiberg, 2003, 2007) concluded that reliable characterization of the exciton–lattice coupling in antenna systems requires a more involved selective spectroscopy technique referred to as differential fluorescence line narrowing (ΔFLN).

Analogous to the hole-burning spectrum, which is obtained as a difference between the pre- and post-burn absorption spectra, the ΔFLN spectrum is a difference between the FLN spectra recorded before and after burning spectral holes. Thus, the ΔFLN spectrum corresponds to the emission of those chromophores that are selectively bleached out between two successive FLN measurements. The main advantage of the ΔFLN method is that it yields almost undistorted ZPLs together with the corresponding phonon structure (see Fig. 4.12), so that electron–phonon and/or exciton–phonon coupling strengths can be determined directly (Rätsep and Freiberg, 2003, 2007). Stabilized lasers and samples of very high optical quality that almost do not scatter light are still required for successful measurements.

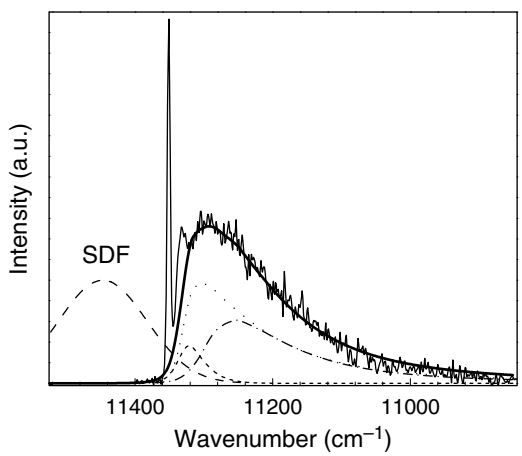

Fig. 4.12. Experimental (thin solid line with noise) ΔFLN spectrum of B800-deficient LH2 complexes from *Rb. sphaeroides* at 5 K. The narrow line at 11,351 cm^{-1} (881 nm) is the ZPL. Its width is limited by the resolution of the experimental setup. The three contributions to the calculated PSB (thick solid line) are: real-PSB (dotted), pseudo-PSB (dash-dotted), and multi-PSB (short dashed). A Gaussian SDF with FWHM equal to 151 cm^{-1} and peak at 11,447 cm^{-1} is represented with dashed line (See text for further details)

Within the basic model that includes adiabatic, harmonic, Condon, and linear electron-phonon coupling approximations, the single site/state fluorescence spectrum at zero temperature of chromophores embedded into an amorphous protein matrix may be written down as (Hayes et al., 1994):

$$L(\nu) = e^{-s} l_0(\nu - \Omega) + \sum_{R=1}^{\infty} S^R \frac{e^{-S}}{R!} l_R(\nu - \Omega + R\nu_m), \quad (4.24)$$

where S is the already defined Huang-Rhys factor. The first term in Eq. (4.24) describes ZPL, while the second one characterizes PSB. The ZPL of shape l_0 peaks at frequency Ω. The l_R-terms with $R = 1, 2, \ldots$ correspond to the one-phonon and multi-phonon transitions. The area-normalized one-phonon spectral profile, $l_1(\nu)$, also called the weighted density of the phonon states, is an important characteristics of dynamical systems that interact with their surroundings. It is a product of two frequency-dependent terms, the density of vibrating states and the electron–phonon coupling strength (Rebane, 1970).

The ΔFLN spectrum in the short burn time limit may be represented as (Pieper et al., 1999):

$$\Delta FLN(\nu) \propto \sum_{R,P=0}^{\infty} \left(S^R \frac{e^{-S}}{R!}\right)\left(S^P \frac{e^{-S}}{P!}\right) \times \int d\Omega N(\Omega - \nu_C)\, l_R\,(\nu - \Omega + R\nu_m) \times l_P(\nu_E - \Omega - P\nu_m)\,. \quad (4.25)$$

Here, $N(\Omega - \nu_c)$ is the Gaussian inhomogeneous site/state distribution function (SDF) centered at ν_C. The ZPL at the excitation frequency ν_E corresponds to the transitions with R, $P = 0$. All other transitions constitute the PSB.[8] The Huang-Rhys factor S is calculated from Eq. (4.26)

[8] Only excitations within the inhomogeneously broadened fluorescence origin band that are resonant with ZPLs are spectrally selective, resulting in line-narrowed FLN spectra. The excitation is nonselective with respect to such sites/states whose fluorescence origin band lies at lower energy than the excitation wavelength, so that the fluorescing state is populated via relaxation. As a result, non-line-

$$e^{-S} = \frac{I_{ZPL}}{I_{ZPL} + I_{real-PSB}} , \qquad (4.26)$$

where I_{ZPL} is the integral intensity of the ZPL and $I_{real-PSB}$, that of the real phonon sideband (real-PSB). The latter term requires an explanation. In selective spectra, including ΔFLN, the intensity of PSB with respect to ZPL is always larger than in the corresponding homogeneously broadened spectrum represented by Eq. (4.24). This is because of two additional contributions, the so-called pseudo-PSB and multi-PSB, which appear in inhomogeneously broadened spectra due to non-resonant excitation via the phonon sidebands[9] (Kikas, 1978; Sapozhnikov and Alekseev, 1984; Pieper et al., 1999; Rätsep and Freiberg, 2003).

Figure 4.12 demonstrates a model analysis of the ΔFLN spectrum for the B800-deficient LH2 complexes at 881-nm excitation. As seen, the real-PSB that according to Eq. (4.26) reports about the exciton–phonon coupling strength constitutes only a bit more than half of the experimental PSB. If the observed PSB was used to calculate the Huang-Rhys factors, instead of the real-PSB much exaggerated value of S would have been obtained. Careful simulations of the experimental spectra are thus required to derive correct model parameters from the selective spectra. Notice that the simplified PSB fit presented in Fig. 4.12 ignores a sharp feature of the experimental sideband of pseudo-local phonon origin shifted by 18–20 cm^{-1} with respect to ZPL.

In relation with Figs. 4.9 and 4.10, reduced efficiency of the selective spectroscopy methods, when applied on the ensembles of LH antennas, was emphasized. Setting up just a single variable, e.g., excitation wavelength, does not guarantee top selectivity. At least two coordinates (excitation energy and the participating ratio/reorganization energy) should in the present model be simultaneously addressed for more complete selection. This is also the key for understanding the fast broadening and loss of structure of the experimental ΔFLN spectra with increasing burn fluence shown in Fig. 4.13.

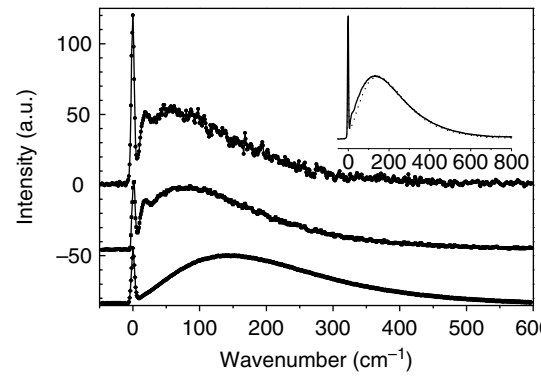

Fig. 4.13. The ΔFLN spectra (two top curves) of the B800-deficient LH2 complexes from *Rb. sphaeroides* at 5 K. The area-normalized spectra are measured at 881 nm with burn fluence of 0.4 J cm^{-2} (*top*) and 21.6 J cm^{-2} (*middle*). The bottom curve is the FLN spectrum recorded after hole burning with fluence of 21.6 J cm^{-2}. The spectra are arbitrarily shifted relative to each other for clarity. The latter FLN spectrum is redrawn with dotted line in the inset to compare with the initial FLN spectrum (black continuous line) before any deliberate hole burning. Notice that in the FLN spectrum the scattered laser line at zero frequency obscures the ZPL

Initially, under low burn fluence, the exciton-like polarons with smallest participation ratio and strongest ZPLs will be burned out, resulting in narrow and structured ΔFLN spectrum. According the fluence buildup, the high-participation-ratio antenna forms, corresponding to self-trapped excitons, start gradually disappear that broadens the remaining spectrum. Because of this burn dependence, all the parameters evaluated from the selective spectra, such as S factors, should be extrapolated to the zero-burn limit. The inset of Fig. 4.13 shows that the FLN spectrum remaining after extensive burning still pretty much reminds the original FLN line shape, except the rather small low-frequency part that has been burned out. These observations suggest that in agreement with Fig. 4.9a the bulk of the excitations generated at the low-energy edge of the absorption spectrum (e.g., at 881 nm) correspond to the dynamically self-trapped excitons.

According to Fig. 4.9a, variations of the FLN spectra with excitation wavelength should appear, the spectra excited at longer wavelength being generally broader (stronger coupled) than those

narrowed (inhomogeneously broadened) fluorescence spectra are obtained.

[9] The terms "resonant" and "nonresonant" are generally used to describe the two contributions to the line-narrowed optical spectra according to the mode of their excitation. Whereas ZPL and real-PSB correspond to the resonant excitation, the pseudo-PSB and multi-PSB constitute the nonresonant parts.

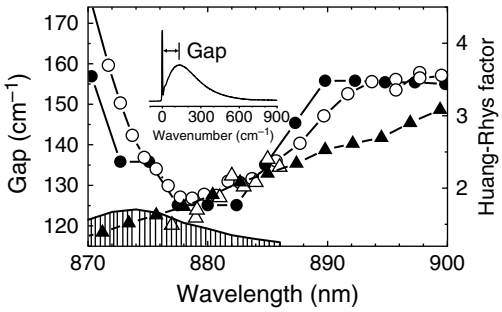

Fig. 4.14. Excitation wavelength dependence of the energy gap (open circles: experiment, filled circles: simulations) and of the Huang-Rhys factor (open triangles: experiment, filled triangles: simulations) in the FLN spectra of B800-deficient LH2 complexes from *Rb. sphaeroides* at 5 K. The energy gap definition is provided in the inset. Sketched with solid vertical lines is the B870 distribution of the spectral hole depths

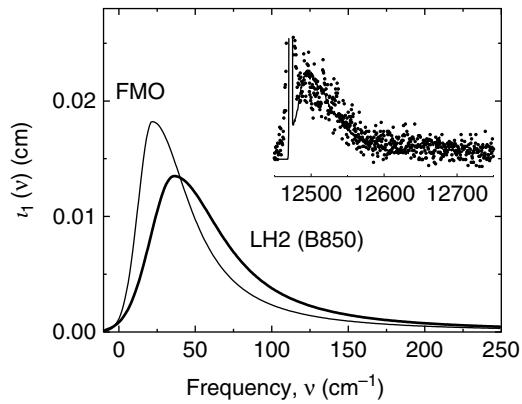

Fig. 4.15. One-phonon functions obtained for the B800-deficient LH2 complexes from *Rb. sphaeroides* (thick solid curve) and for the FMO complexes from *Chlorobium tepidum* (thin solid curve). The inset compares the low-temperature sidebands in the fluorescence excitation spectrum of a B800 molecule in a single LH2 complex from *Rs. molishianum* (scatter) (Hofmann et al., 2005) and in the ΔFLN spectrum of the FMO complexes (continuous line) (Rätsep and Freiberg, 2007). To achieve the overlap the ZPL at 827.1 nm in the FMO spectrum was shifted until it coincided with the origin of the single molecule spectrum and then its x-axis was reversed

measured at shorter wavelengths. Figure 4.14, where excitation wavelength dependence of the gap (as defined in the inset) and the Huang-Rhys factor is shown for the B800-deficient LH2 complexes, fully confirms these expectations. The gap, a measure of the reorganization energy, havings a minimum value of $\sim$127 cm^{-1} at 878 nm. It increases toward longer wavelengths until becoming saturated at $\sim$157 cm^{-1} above 894 nm.[10] Where comparison is available (experimental evaluation of the factors from the FLN spectra is technically limited by the ability to burn well-defined spectral holes), the experimental and model behaviors of the gap and are similar. The exciton–phonon coupling is strong because the Huang-Rhys factor is greater than 1 over the whole spectral range available to the measurements. As seen, the simulations predict that S may reach 3 or even greater values at the far-red edge of the spectrum. A reasonable fit was achieved with ν_m in the range of 40–50 cm^{-1}. In Section V. A mean frequencies around 30–40 cm^{-1} were used. It is worth noticing that with all these frequencies the adiabatic approximation of the Holstein model is well obeyed, since $\nu_m / V \approx (40\text{–}50)/370 \ll 1$.

The selective spectroscopy model described, in principle, allows the one-phonon profile, $l_1(\nu)$, to be recovered from experimental spectra. A solution of such inverse problem for the B800-deficient LH2 complexes is shown in Fig. 4.15.[11] Exposed also in this figure is the similarly computed profile for the FMO antenna complex. It is a generally believed that a single Bchl molecule is responsible for the fluorescence emission of the FMO complex. This indeed might be the case because, as demonstrated in the inset, the shape of the PSB in the FMO emission spectrum almost coincides with the PSB in the fluorescence excitation spectrum of quasi-monomeric B800 molecules in the LH2 complex from *Rs. molishianum*, measured in a single molecule experiment (Hofmann et al., 2005). The FMO spectrum thus provides a reference one-phonon spectrum of a single Bchl molecule locally coupled to protein environment.

[10] An increase of the gap below 878 nm is due to the excitation energy relaxation as explained above and has no relevance to the exciton–phonon coupling change, our main concern here.

[11] Let us notice again (see remark at Fig. 4.12) that for simplicity the pseudo-local phonon feature of the experimental spectrum has been ignored in these simulations.

As can be seen from Fig. 4.15, the two profiles differ considerably. The one-phonon spectrum of B850 is much broader than that of FMO (FWHM equal to $58\,cm^{-1}$ and $41\,cm^{-1}$, respectively) with its peak at almost twice higher frequency ($36\,cm^{-1}$ and $22\,cm^{-1}$, respectively). To the extent that the FMO spectrum represents the true local response of the protein to the electronic transition in every single Bchl molecule, these differences could be associated with assembly of the Bchl molecules into the B850 aggregate. Let us notice that the peak phonon energy is generally smaller than the energy gap between the adjacent exciton states of the B850 aggregate at the lower Davydov subband region ($\sim 100\,cm^{-1}$ (Wu et al., 1997b; Freiberg et al., 1999; Van Oijen et al., 1999)). This validates the selective excitation approximation discussed in Section IV.A.

The knowledge of the one-phonon profile and the Huang-Rhys factor (i.e., the spectral density function) provides a method for calculation of the reorganization energy of the excitonic polarons according to Eq. (4.27):

$$\lambda_0 = hS \int_0^\infty d\nu l_1(\nu)\nu. \qquad (4.27)$$

Taking $S = 1.6$ for the B850 aggregate and $S = 0.4$ for the FMO complex (those are the Huang-Rhys factor values at half height of the corresponding SDFs (see Fig. 4.14 and reference Rätsep and Freiberg, 2007), the reorganization energies of $128\,cm^{-1}$ and $25\,cm^{-1}$, respectively, were obtained by integration between 0 and $500\,cm^{-1}$. In the case of FMO, one is justified to write $\lambda_0^{FMO} \equiv E_{LR}^{FMO}$. In reference (Adolphs and Renger, 2006), the same feature was calculated equal to $40\,cm^{-1}$. The much bigger site reorganization energy of $E_{LR}^{B850} = 190\,cm^{-1}$ found for the Bchls in the B850 complex of B800-deficient LH2 complexes from the anisotropy simulations (see Table 4.1) is qualitatively consistent with the basic idea followed in this work that excitons in the tightly packed antenna aggregates are rather strongly coupled to the environment. In this regard, it is worth noticing that the surroundings of the aggregated Bchls include both the protein subunits and the neighboring pigments, differently from the lone Bchl in the FMO complex hosted just by the protein. Since $L_0 = E_{LR}/\lambda_0$ (see Eq. 4.18), one gets $L_0 \approx 1.4$, the value which is within the standard deviation of calculated sizes of the excitonic polarons at $g = 0.3$ (Fig. 4.8b).

VI. Conclusions and Outlook

In this chapter, the origin of the electronic excited states in the ring-shaped bacteriochlorophyll aggregates has been studied by theoretical analysis and numerical evaluation of various spectroscopic parameters characterizing these states. Such aggregates govern the functionally important ultrafast funneling of the solar excitation energy in the photosynthetic membranes of purple bacteria. The optical spectroscopy data of LH1 and LH2 antenna complexes acquired at low temperatures when the quantum aspects of the material excitations dominate were investigated in terms of collective (exciton and excitonic polaron) quantum eigenstates. The limited size and the known spatial structure of the aggregates greatly support such detailed analysis. On broader molecular physics vista, these aggregates may be considered as unique model systems of a 1D topology having fixed (genetically predetermined) size with practically zero dispersion.

We have shown that the absorbing and the emitting electronic states of the antenna aggregates could not be adequately described within the common disordered Frenkel exciton approach. This is understandable since in 1D molecular arrays already infinitesimal couplings between the exciton and the bath of vibrational modes (that in the antenna pigment-protein complexes involve movements of both the protein and the pigment atoms) develop excitonic polarons and/or self-trapped excitons with nonuniform displacement of the nuclear coordinates. The Holstein Hamiltonian has been applied for characterization of steady-state eigenstates of the excitonic polarons is 1D systems. To analyze real situations, static disorder should be included. Despite apparent simplicity of such a model, its quantitative evaluation in the case of the B850 and B875 aggregates happened to be challenging. This is because the energetic parameters that govern the electronic structure and the dynamics of the antenna excitations

such as σ, V, E_{LR} are all of the same order of magnitude. Also, new effects distinct from those in the regular 1D systems appear. At exciton–phonon couplings above some critical strength, the disordered antenna aggregates may support multiple self-trapped excitons with different size, reorganization energy, and spatial location. In certain sense they become similar to the 2D and 3D ordered systems where free excitons coexist with the self-trapped excitons, separated by an energy barrier. Yet, the excitons in disordered 1D aggregates are always to some extent localized by static disorder. Attracted by the low energy sites of the lattice they can further dynamically localize by the self-trapping mechanism. The critical exciton–phonon coupling value for the coexistence depends on particular disorder realization.

Exciton self-trapping generally results in broadened and Stokes shifted fluorescence spectra, potentially improving efficiency of the incoherent energy transfer between the antenna complexes. Furthermore, at $g \approx 0.3$ and $\sigma \approx 0.6V$, appropriate numbers for the B850 aggregate, the emission rate is at the highest possible value, being a couple of times larger than that for disordered Frenkel excitons. This notable amplification of the emission rate might also have photosynthetic relevance by optimizing energy transport and trapping processes. It was recently proposed (Markvart and Greef, 2004) that the incoherent Förster energy transfer mechanism and the thermally activated transport of self-trapped excitonic polarons are closely related. Efforts are still required to explicitly demonstrate this idea on clusters of antenna complexes and on complete photosynthetic membranes.

The excitonic polaron model presented in this chapter for the first time allows a consistent description of the low-temperature absorption and emission spectra of bacterial antennas. The spectra measured at physiological temperatures generally require more sophisticated analysis based on density matrix methods (see e.g. Van Grondelle and Novoderezhkin, 2006; Urboniene et al., 2007). However, recent studies (Schröder et al., 2006) of the LH2 complexes using non-Markovian as well as modified Redfield approaches have demonstrated that it is difficult to choose between the various dynamic models, as their differences are smeared out by ensemble average. Therefore, the energetic parameters obtained at low temperatures are very valuable for the calibration of various dynamic theories.

Acknowledgments

This work was partially supported by the Estonian Science Foundation grant No. 7002. The authors are grateful to M. Rätsep, K. Timpmann, and L. Valkunas for useful comments. Rätsep and Timpmann also provided experimental data for Figs. 4.11–4.15. J. Köhler kindly made available the single molecule spectrum shown in the inset of Fig. 4.15.

References

Adolphs J and Renger T (2006) How proteins trigger energy transfer in the FMO complex of green sulfur bacteria. Biophys J 91: 2778–2797

Agarwal R, Rizvi AH, Prall BS, Olsen JD, Hunter CN and Fleming GR (2002) Nature of disorder and inter-complex energy transfer in LH2 at room temperature: A three photon echo peal shift study. J Phys Chem A 106: 7573–7578

Amunts A, Drory O and Nelson N (2007) The structure of a plant photosystem I supercomplex at 3.4 A resolution. Nature 447: 58–63

Bahatyrova S, Frese RN, Van der Werf KO, Otto C, Hunter CN and Olsen JD (2004) Flexibility and size heterogeneity of the LH1 light harvesting complex revealed by atomic force microscopy. J Biol Chem 279: 21327–21333

Beekman LMP, Van Mourik F, Jones MR, Visser HM, Hunter CN and Van Grondelle R (1994) Trapping in mutants of the photosynthetic purple bacterium *Rhodobacter sphaeroides*: Influence of the charge separation rate and consequences for the rate-limiting step in the light-harvesting process. Biochemistry 33: 3143–3147

Borisov AY and Godik VI (1972) Energy transfer in bacterial photosynthesis. I. Light intensity dependences of fluorescence lifetimes. J Bioenerg 3: 211–220

Borisov AY, Freiberg AM, Godik VI, Rebane K and Timpmann K (1985) Kinetics of picosecond bacteriochlorophyll luminescence in vivo as a function of the reaction center state. Biochim Biophys Acta 807: 221–229

Cogdell RJ, Gall A and Köhler J (2006) The architecture and function of the light-harvesting apparatus of purple bacteria: From single molecules to in vivo membranes. Quart Rev Biophys 39: 227–324

Cruzeiro-Hansson L, Eilbeck JC, Marin JL and Russell FM (2000) Interplay between dispersive and non-dispersive modes in the polaron problem. Phys Lett A 266: 160–166

Dahlbom M, Pullerits T, Mukamel S and Sundstrom V (2001) Exciton delocalization in the B850 light-harvesting complex: Comparison of different measures. J Phys Chem B 105: 5515–5524

Damjanovic A, Kosztin I, Kleinekathöfer U and Schulten K (2002) Excitons in a photosynthetic light-harvesting system: A combined molecular dynamics, quantum chemistry, and polaron model study. Phys Rev E 65: 031919–031943

Davydov AS (1971) Theory of Molecular Excitons. Plenum Press, New York

Dobek A, Deprez J, Paillotin G, Leibl W, Trissl HW and Breton J (1990) Excitation trapping efficiency and kinetics in *Rb. sphaeroides* R26.1 whole cells probed by photovoltage measurements on the picosecond time-scale. Biochim Biophys Acta 1015: 313–321

Duysens LNM (1952) PhD Thesis: Transfer of Excitation Energy in Photosynthesis. State University, Utrecht

Duysens LNM (1986) Introduction to (bacterio) chlorophyll emission: A historical perspective. In: Govindjee, Amesz J and Fork DC (eds) Light Emission by Plants and Bacteria, pp 3–28. Academic, Orlando, FL

Emerson R and Arnold WA (1932) The photochemical reaction in photosynthesis. J Gen Physiol 16: 191–205

Emin D and Bussac M-N (1994) Disorder-induced small-polaron formation. Phys Rev B 49: 14290–14300

Fenna RE and Matthews BW (1975) Chlorophyll arrangement in a bacteriochlorophyll protein from *Chlorobium limicola*. Nature 258: 573–577

Fetisova ZG (2004) Survival strategy of photosynthetic organisms. 1. Variability of the extent of light-harvesting pigment aggregation as a structural factor optimizing the function of oligomeric photosynthetic antenna. Model calculations. Mol Biol 38: 434–440

Fetisova ZG, Borisov AY and Fok MV (1985) Analysis of structure-function correlations in light-harvesting photosynthetic antenna: Structure optimization parameters. J Theor Biol 112: 41–75

Fetisova ZG, Freiberg A and Timpmann K (1988) Long-range molecular order as an efficient strategy for light harvesting in photosynthesis. Nature 334: 633–634

Fetisova ZG, Shibaeva LV and Fok MV (1989) Biological expedience of oligomerization of chlorophyllous pigments in natural photosynthetic systems. J Theor Biol 140: 167–184

Fetisova ZG, Shibaeva LV and Taisova AS (1995) Oligomerization of light-harvesting pigments as a structural factor optimizing photosynthetic antenna function. I. Model calculations. Mol Biol (Moscow) 29: 1384–1390

Fidder H, Knoester J and Wiersma DA (1991) Optical properties of disordered molecular aggregates: A numerical study. J Chem Phys 95: 7880–7890

Franck J and Teller E (1938) Migration and photochemical action of excitation energy in crystals. J Chem Phys 6: 861–872

Freiberg A (1995) Coupling of antennas to reaction centers. In: Blankenship RE, Madigan MT and Bauer CE (eds) Anoxygenic Photosynthetic Bacteria, pp 385–398. Kluwer, Dordrecht, The Netherlands

Freiberg A, Godik VI and Timpmann K (1984) Excitation energy transfer in bacterial photosynthesis studied by picosecond laser spectrochronography. In: Sybesma C (ed) Advances in Photosynthesis Research, pp 45–48. Nijhoff, Hague, The Netherlands

Freiberg A, Godik VI and Timpmann K (1987) Spectral dependence of the fluorescence lifetime of *Rhodospirillum rubrum*. Evidence for inhomogeneity of B880 absorption band. In: Biggins J (ed) Progress in Photosynthesis Research, pp 45–48. Nijhoff, Dordrecht, The Netherlands

Freiberg A, Godik VI, Pullerits T and Timpmann KE (1988) Directed picosecond excitation transport in purple photosynthetic bacteria. Chem Phys 128: 227–235

Freiberg A, Godik VI, Pullerits T and Timpman K (1989) Picosecond dynamics of directed excitation transfer in spectrally heterogeneous light-harvesting antenna of purple bacteria. Biochim Biophys Acta 973: 93–104

Freiberg A, Allen JP, Williams J and Woodbury NW (1996) Energy trapping and detrapping by wild type and mutant reaction centers of purple non-sulfur bacteria. Photosynth Res 48: 309–319

Freiberg A, Jackson JA, Lin S and Woodbury NW (1998a) Subpicosecond pump-supercontinuum probe spectroscopy of LH2 photosynthetic antenna proteins at low temperature. J Phys Chem A 102: 4372–4380

Freiberg A, Timpmann K, Lin S and Woodbury NW (1998b) Exciton relaxation and transfer in the LH2 antenna network of photosynthetic bacteria. J Phys Chem B 102: 10974–10982

Freiberg A, Timpmann K, Ruus R and Woodbury NW (1999) Disordered exciton analysis of linear and nonlinear absorption spectra of antenna bacteriochlorophyll aggregates: LH2-only mutant chromatophores of *Rhodobacter sphaeroides* at 8 K under spectrally selective excitation. J Phys Chem B 103: 10032–10041

Freiberg A, Rätsep M, Timpmann K and Trinkunas G (2003a) Self-trapped excitons in circular bacteriochlorophyll antenna complexes. J Luminescence 102–103: 363–368

Freiberg A, Rätsep M, Timpmann K, Trinkunas G and Woodbury NW (2003b) Self-trapped excitons in LH2 antenna complexes between 5 K and ambient temperature. J Phys Chem B 107: 11510–11519

Godik VI and Borisov AY (1977) Excitation trapping by different states of photosynthetic reaction centers. FEBS Lett 82: 355–358

Godik VI, Freiberg A, Timpmann K, Borisov AY and Rebane K (1987) Picosecond excitation energy transfer between different light-harvesting complexes and reaction centers in purple bacteria. In: Biggins J (ed) Progress in Photosynthesis Research, pp 41–44. Nijhoff, Dordrecht, The Netherlands

Godik VI, Timpmann KE and Freiberg AF (1988) Spectral inhomogeneity of the bacteriochlorophyll absorption band of *Rhodospirillum rubrum* as studied by picosecond fluorescence spectroscopy. Dokl Akad Nauk SSSR 298: 1469–1473

Gooijer C, Ariese F and Hofstraat JW (2000) Shpol'skii Spectroscopy and Other Site-Selective Methods. Wiley, New York, USA

Green BR and Parson WW (eds) (2003) Ligh-Harvesting Antennas in Photosynthesis. Kluwer, Dordrecht/Boston, MA/ London

Hayes JM, Lyle PA and Small GJ (1994) A theory for the temperature dependence of hole-burned spectra. J Phys Chem 98: 7337–7341

Heijs DJ, Malyshev VA and Knoester J (2005) Decoherence of excitons in multichromophore systems: Thermal line broadening and destruction of superradiant emission. Phys Rev Lett 95: 177402

Hofmann C, Michel H, Van Heel M and Köhler J (2005) Multivariate analysis of single-molecule spectra: Surpassing spectral diffusion. Phys Rev Lett 94: 195501

Holstein T (1959) Studies of polaron motion. Part I. The molecular-crystal model. Ann Phys 8: 325–342

Hu X, Ritz T, Damjanovic A, Autenrieth F and Schulten K (2002) Photosynthetic apparatus of purple bacteria. Quart Rev Biophys 35: 1–62

Jang S, Dempster SE and Silbey RJ (2001) Characterization of the static disorder in the B850 of LH2. J Phys Chem B 2001: 6655–6665

Jimenez R, Dikshit SN, Bradforth SE and Fleming GR (1996) Electronic excitation transfer in the LH2 complex of *Rhodobacter sphaeroides*. J Phys Chem 100: 6825–6834

Kabanov VV and Mashtakov OY (1993) Electron localization with and without barrier formation. Phys Rev B 47: 6060–6064

Karrasch S, Bullough PA and Ghosh R (1995) The 8.5 A projection map of the light-harvesting complex I from *Rhodospirillum rubrum* reveals a ring composed of 16 subunits. EMBO J 14: 631–368

Katiliene Z, Katilius E, Uyeda G, Williams J-AC and Woodbury NW (2004) Increasing the rate of energy transfer between the LH1 antenna and the reaction center in the photosynthetic bacterium *Rhodobacter sphaeroides*. J Phys Chem B 108: 3863–3870

Kikas J (1978) Effects of inhomogneity and site selective impurity-phonon coupling in solid solutions. Chem Phys Lett 57: 511–513

Knox RS (1963) Theory of Excitons. Academic, New York

Koepke J, Hu X, Muenke C, Schulten K and Michel H (1996) The crystal structure of the light-harvesting complex II (B800–850) from *Rhodospirillum molischianum*. Structure 4: 581–597

Koolhaas MHC, Van der Zwan G, Frese RN and Van Grondelle R (1997) Red shift of the zero crossing in the CD spectra of the LH2 antenna complex of *Rhodopseudomonas acidophila*: A structure-based study. J Phys Chem B 101: 7262–7270

Kramer HJM, Van Grondelle R, Hunter CN, Westerhuis WHJ and Amesz J (1984) Pigment organization of the B800–850 antenna complex of *Rhodopseudomonas sphaeroides*. Biochim Biophys Acta 765: 156–165

Leggett AJ, Chakravarty S, Dorsey AT, Fischer MPA, Garg A and Zwerger W (1987) Dynamics of the dissipative two-state system. Rev Mod Phys 59: 1–85

Liuolia V, Valkunas L and Van Grondelle R (1997) Excitons in dimerized chains. J Phys Chem B 101: 7343–7349

Loll B, Kern J, Saenger W, Zouni A and Biesiadka J (2005) Towards complete cofactor arrangement in the 3.0 A resolution structure of photosystem II. Nature 438: 1040–1044

Lu N and Mukamel S (1991) Polaron and size effects in optical lineshapes of molecular aggregates. J Chem Phys B 95: 1588–1607

Markvart T (2000) Light harvesting for quantum solar conversion. Prog Quant Electr 24: 107–186

Markvart T and Greef R (2004) Polaron-exciton model of resonance energy transfer. J Chem Phys 121: 6401–6405

Matsui A, Mizuno K and Nishimura H (1984) Zero-phonon kines associated with self-trapped exciton states and exciton dynamics in β-perylene. J Phys Soc Jpn 53: 2818–2827

McDermott G, Prince SM, Freer AA, Hawthornthwaite-Lawless AM, Papiz MZ, Cogdell RJ and Isaacs NW (1995) Crystal structure of an integral membrane light-harvesting complex from photosynthetic bacteria. Nature 374: 517–521

McLuskey K, Prince SM, Cogdell RJ and Isaacs NW (2001) The crystallographic structure of the B800–820 LH3 light-harvesting complex from the purple bacteria *Rhodopseudomonas acidophila* stain 7050. Biochemistry 40: 8783–8789

Meier T, Zhao Y, Chernyak V and Mukamel S (1997) Polarons, localization, and excitonic coherence in superradiance of biological antenna complexes. J Chem Phys 107: 3876–3893

Michel H and Deisenhofer J (1990) The photosynthetic reaction center from the purple bacterium *Rhodopseudomonas viridis*: aspects of membrane protein structure. Curr Top Membr Transp 36: 53–69

Monshouwer R, Visschers RW, Van Mourik F, Freiberg A and Van Grondelle R (1995) Low-temperature absorption and site-selected fluorescence of the light-harvesting antenna of *Rhodopseudomonas viridis*. Evidence for heterogeneity. Biochim Biophys Acta 1229: 373–380

Monshouwer R, Abrahamsson M, Van Mourik F and Van Grondelle R (1997) Superradiance and exciton delocalization in bacterial photosynthetic light-harvesting systems. J Phys Chem B 101: 7241–7248

Mukamel S (1995) Principles of Nonlinear Optical Spectroscopy. Oxford/New York

Noba K and Kayanuma Y (1998) Numerically rigorous results for the ground stsate of exciton-lattice systems. J Phys Soc Jpn 67: 3972–3975

Novoderezhkin VI and Razjivin AP (1993) Excitonic interactions in the light-harvesting antenna of photosynthetic purple bacteria and their influence on picosecond absorbance difference spectra. FEBS Lett 330: 5–7

Novoderezhkin VI and Razjivin AP (1995) Exciton dynamics in circular aggregates: application to antenna of photosynthetic purple bacteria. Biophys J 68: 1089–1100

Novoderezhkin V, Monshouwer R and Van Grondelle R (1999) Disordered exciton model for the core light-harvesting antenna of *Rhodopseudomonas viridis*. Biophys J 77: 666–681

Nuijs AM, Van Grondelle R, Joppe HLP, Cees Van Bochove A and Duysens LNM (1986) A picosecond-absorption study on bacteriochlorophyll excitation, trapping and primary-charge separation in chromatophores of *Rhodospirillum rubrum*. Biochim Biophys Acta 850: 286–293

Papiz MZ, Prince SM, Howard T, Cogdell RJ and Isaacs NW (2003) The structure and thermal motion of the B800–850 LH2 complex from *Rps. acidophila* at 2.0 A resolution at 100 K: New structural features and functionally relevant motions. J Mol Biol 326: 1523–1538

Pearlstein RM (1982) Exciton migration and trapping in photosynthesis. Photochem Photobiol 35: 835–844

Pieper J, Voigt J, Renger G and Small GJ (1999) Analysis of phonon structure in line-narrowed optical spectra. Chem Phys Lett 310: 296–302

Porter G, Tredwell CJ, Searle GFW and Barber J (1978) Picosecond time-resolved energy transfer in Porphyrindum cruentum. Biochim Biophys Acta 501: 232–245

Pullerits T and Freiberg A (1991) Picosecond fluorescence of simple photosynthetic membranes: evidence of spectral inhomogeneity and directed energy transfer. Chem Phys 149: 409–418

Pullerits T, Visscher KJ, Hees S, Sundstroem V, Freiberg A, Timpmann K and Van Grondelle R (1994) Energy transfer in the inhomogeneously broadened core antenna of purple bacteria: a simultaneous fit of low-intensity picosecond absorption and fluorescence kinetics. Biophys J 66: 236–248

Rashba IE (1982) Self-trapping of excitons. In: Sturge MD (ed) Excitons, pp 543–602. North-Holland, Amsterdam

Rätsep M and Freiberg A (2003) Resonant emission from the B870 exciton state and electron-phonon coupling in the LH2 antenna chromoprotein. Chem Phys Lett 377: 371–376

Rätsep M and Freiberg A (2007) Electron-phonon and vibronic couplings in the FMO bacteriochlorophyll a antenna complex studied by difference fluorescence line narrowing. J Luminescence 127: 251–259

Rätsep M, Hunter CN, Olsen JD and Freiberg A (2005) Band structure and local dynamics of excitons in bacterial light-harvesting complexes revealed by spectrally selective spectroscopy. Photosynth Res 86: 37–48

Rebane KK (1970) Impurity Spectra of Solids. Plenum Press, New York

Reddy NRS, Picorel R and Small GJ (1992) B896 and B870 components of the *Rhodobacter sphaeroides* antenna: A hole burning study. J Phys Chem 96: 6458–6464

Renger T and Marcus RA (2002) On the relation of protein dynamics and exciton relaxation in pigment-protein complexes: An estimation of the spectral density and a theory for the calculation of optical spectra. J Chem Phys 116: 9997–10019

Robinson GW (1967) Excitation transfer and trapping in photosynthesis. Brookhaven Symp Biol 19: 16–48

Romero AH, Brown DW and Lindenberg K (1999) Effects of dimensionality and anisotropy on the Holstein polaron. Phys Rev B 60: 14080–14091

Roszak AW, Howard TD, Southall J, Gardiner AT, Law CJ, Isaacs NW and Cogdell RJ (2003) Crystal structure of the RC-LH1 core complex from *Rhodopseudomonas palustris*. Science 302: 1969–1972

Sapozhnikov MN and Alekseev VI (1984) Site selective luminescence spectroscopy of impurity centres in solids: Model calculations and experiment. Chem Phys Lett 107: 265–271

Sauer K and Austin LA (1978) Bacteriochlorophyll-protein complexes from the light-harvesting antenna of photosynthetic bacteria. Biochemistry 17: 2011–2019

Sauer K, Cogdell RJ, Prince SM, Freer A, Isaacs NW and Scheer H (1996) Structure-based calculations of the optical spectra of the LH2 bacteriochlorophyll-protein complex from *Rhodopseudomonas acidophila*. Photochem Photobiol 64: 564–576

Scherz A and Parson WW (1986) Interactions of the bacteriochlorophylls in antenna bacteriochlorophyll-protein complexes of photosynthetic bacteria. Photosynth Res 9: 21–32

Scheuring S (2006) AFM studies of the supramolecular assembly of bacterial photosynthetic core-complexes. Curr Opin Chem Biol 10: 387–393

Scholes GD (2003) Long-range resonance energy transfer in molecular systems. Annu Rev Phys Chem 54: 57–87

Scholes GD and Fleming GR (2000) On the mechanism of light harvesting in photosynthetic purple bacteria: B800 to B850 energy transfer. J Phys Chem B 104: 1854–1868

Scholes GD and Rumbles G (2006) Excitons in nanoscale systems. Nat Mater 5: 683–693

Scholes GD, Harcourt RD and Fleming GR (1997) Electronic interactions in photosynthetic light-harvesting complexes: The role of carotenoids. J Phys Chem B 101: 7302–7312

Scholes GD, Gould IR, Cogdell RJ and Fleming GR (1999) Ab initio molecular orbital calculations of electronic couplings in the LH2 bacterial ligh-harvesting complex of *Rps. acidophila*. J Phys Chem B 103: 2543–2553

Schröder M, Kleinekathöfer U and Schreiber M (2006) Calculation of absorption spectra for light-harvesting systems using non-Markovian approaches as well as modified Redfield theory. J Chem Phys 124: 084903

Sebban P and Moya I (1983) Fluorescence lifetime spectra of in vivo bacteriochlorophyll at room temperature. Biochim Biophys Acta 722: 436–442

Sebban P, Jolchine G and Moya I (1984) Spectra of fluorescence lifetime and intensity of Rhodopseudomonas sphaeroides at room and low temperature. Comparison between the wild type, the C 71 reaction center-less mutant and the B800–850 pigment-protein complex. Photochem Photobiol 39: 247–253

Shreve AP, Trautman JK, Frank HA, Owens TG and Albrecht AC (1991) Femtosecond energy-transfer processes in the B800–850 light-harvesting complex of *Rhodobacter sphaeroides* 2.4.1. Biochim Biophys Acta 1058: 280–288

Song KS and Williams RT (1992) Self-Trapped Excitons. Springer, Berlin/Heidelberg/New York

Stoneham AM, Gavartin J, Shluger AL, Kimmel AV, Mũnoz Ramo D, Rønnow HM, Aeppli G and Renner C (2007) Trapping, self-trapping and the polaron family. J Phys: Condens Matter 19: 255208

Sumi H (1994) Two types of self-trapped states for excitons in one dimension. J Phys Soc Jpn 63: 4489–4498

Sumi H (1999a) Theory of rapid excitation-energy transfer from B800 to optically-forbbiden exciton states of B850 in the antenna system LH2 of photosynthetic purple bacteria. J Phys Chem B 103: 6096–6102

Sumi H (1999b) Theory of rates of excitation-energy transfer between molecular aggregates through distributed transition dipoles with application to the antenna system in bacterial photosynthesis. J Phys Chem B 103: 252–260

Sumi H (2000) Bacterial photosynthesis begins with quantum-mechanical coherence. Chem Rec 1: 480–493

Sundström V, Van Grondelle R, Bergstroem H, Aakesson E and Gillbro T (1986) Excitation-energy transport in the bacteriochlorophyll antenna systems of *Rhodospirillum rubrum* and *Rhodobacter sphaeroides*, studied by low-intensity picosecond absorption spectroscopy. Biochim Biophys Acta 851: 431–446

Sundström V, Pullerits T and Van Grondelle R (1999) Photosynthetic light-harvesting: Reconciling dynamics and structure of purple bacterial LH2 reveals function of photosynthetic unit. J Phys Chem B 103: 2327–2346

Tanaka S (2003) Ultrafast relaxation dynamics of the one-dimensional molecular chain: The time-resolved spontaneous emission and exciton coherence. J Chem Phys 119: 4891–4904

Tietz C, Chekhlov O, Dräbenstedt A, Schuster J and Wrachtrup J (1999) Spectroscopy on single light-harvesting complexes at low temperature. J Phys Chem B 103: 6328–6333

Timpmann K, Zhang FG, Freiberg A and Sundström V (1993) Detrapping of excitation energy from the reaction center in the photosynthetic purple bacterium *Rhodospirillum rubrum*. Biochim Biophys Acta 1183: 185–193

Timpmann K, Freiberg A and Sundström V (1995) Energy trapping and detrapping in the photosynthetic bacterium *Rhodopseudomonas viridis*: transfer-to-trap-limited dynamics. Chem Phys 194: 275–283

Timpmann K, Katiliene Z, Woodbury NW and Freiberg A (2001) Exciton self-trapping in one-dimensional photosynthetic antennas. J Phys Chem B 105: 12223–12225

Timpmann K, Rätsep M, Hunter CN and Freiberg A (2004a) Emitting excitonic polaron states in core LH1 and peripheral LH2 bacterial light-harvesting complexes. J Phys Chem B 108: 10581–10588

Timpmann K, Trinkunas G, Olsen JD, Hunter CN and Freiberg A (2004b) Bandwidth of excitons in LH2 bacterial antenna chromoproteins. Chem Phys Lett 398: 384–388

Timpmann K, Trinkunas G, Qian P, Hunter CN and Freiberg A (2005) Excitons in core LH1 antenna complexes of photosynthetic bacteria: Evidence for strong resonant coupling and off-diagonal disorder. Chem Phys Lett 414: 359–363

Trinkunas G and Freiberg A (2005) Abrupt exciton self-trapping in finite and disordered one-dimensional aggregates. J Luminescence 112: 420–423

Trinkunas G and Freiberg A (2006) A disordered polaron model for polarized fluorescence excitation spectra of LH1 and LH2 bacteriochlorophyll antenna aggregates. J Luminescence 119–120: 105–110

Ueta M, Kanzaki H, Kobayashi K, Toyozawa Y and Hanamura E (1986) Excitonic Processes in Solids. Springer, Berlin

Urboniene V, Vrublevskaja O, Gall A, Trinkunas G, Robert B and Valkunas L (2005) Temperature broadening of LH2 absorption in glycerol solution. Photosynth Res 86: 49–59

Urboniene V, Vrublevskaja O, Trinkunas G, Gall A, Robert B and Valkunas L (2007) Solvation effect of bacteriochlorophyll excitons in light-harvesting complex LH2. Biophys J 93: 2188–2198

Van Amerongen H, Valkunas L and Van Grondelle R (2000) Photosynthetic Excitons. World Scientific, Singapore

Van der Laan H, Schmidt T, Visschers RW, Visscher KJ, Van Grondelle R and Volker S (1990) Energy transfer in the B800–850 antenna complex of purple bacteria *Rhodobacter sphaeroides*: a study by spectral hole-burning. Chem Phys Lett 170: 231–238

Van Grondelle R and Novoderezhkin VI (2006) Energy transfer in photosynthesis: experimental insights and quantitative models. Phys Chem Chem Phys 8: 793–807

Van Grondelle R, Bergström H, Sundström V and Gillbro T (1987) Energy transfer within the bacteriochlorophyll antenna of purple bacteria at 77 K, studied by picosecond absorption recovery. Biochim Biophys Acta 894: 313–326

Van Mourik F, Visschers RW and Van Grondelle R (1992) Energy transfer and aggregate size effects in the

inhomogeneously broadened core light-harvesting complex of *Rhodobacter sphaeroides*. Chem Phys Lett 193: 1–7

Van Oijen AM, Ketelaars M, Köhler J, Aartsma TJ and Schmidt J (1998) Spectroscopy of single light-harvesting complexes from purple photosynthetic bacteria at 1.2 K. J Phys Chem B 102: 9363–9366

Van Oijen AM, Ketelaars M, Köhler J, Aartsma TJ and Schmidt J (1999) Unraveling the electronic structure of individual photosynthetic pigment-protein complexes. Science 285: 400–402

Visschers RW, Germeroth L, Michel H, Monshouwer R and Van Grondelle R (1995) Spectroscopic properties of the light-harvesting complexes from *Rhodospirillum molischianum*. Biochim Biophys Acta 1230: 147–154

Vredenberg WJ and Duysens LMN (1963) Transfer of energy from bacteriochlorophyll to a reaction centre during bacterial photosynthesis. Nature 4865: 355–357

Walz T, Jamieson SJ, Bowers CM, Bullough PA and Hunter CN (1998) Projection structures of three photosynthetic complexes from *Rhodobacter sphaeroides*: LH2 at 6 A, LH1 and RC-LH1 at 25 A. J Mol Biol 282: 833–845

Wu H-M and Small GJ (1998) Symmetry-based analysis of the effects of random energy disorder on the excitonic level structure of cyclic arrays: Application to photosynthetic antenna complexes. J Phys Chem B 102: 888–898

Wu H-M, Rätsep M, Jankowiak R, Cogdell RJ and Small GJ (1997a) Comparison of the LH2 antenna complexes of *Rhodopseudomonas acidophila* (strain 10050) and *Rhodobacter sphaeroides* by high-pressure absorption, high-pressure hole burning, and temperature-dependent absorption spectroscopies. J Phys Chem B 101: 7641–7653

Wu H-M, Rätsep M, Lee I-J, Cogdell RJ and Small GJ (1997b) Exciton level structure and energy disorder of the B850 ring of the LH2 antenna complex. J Phys Chem B 101: 7654–7663

Zhang FG, Van Grondelle R and Sundström V (1992) Pathways of energy flow through the light-harvesting antenna of the photosynthetic purple bacterium *Rhodobacter sphaeroides*. Biophys J 61: 911–920